Characterizing the potential for fault reactivation related to fluid injection through subsurface structural mapping and stress field analysis, Wellington Field, Sumner County, KS

By

Drew R. Schwab

Submitted to the graduate degree program in Geology and the Graduate Faculty of the University of Kansas in partial fulfillment of the requirements for the degree of Master of Science.

_____

Chairperson, Dr. Tandis S. Bidgoli

_____

Co-Chairperson, Dr. Michael H. Taylor

_____

Dr. Leigh A. Stearns

Date Defended: December 9, 2016

The thesis committee for Drew Schwab

certifies that this is the approved version of the following thesis:

Characterizing the potential for fault reactivation related to fluid injection through subsurface structural mapping and stress field analysis, Wellington Field, Sumner County, KS

_____

Chairperson, Dr. Tandis S. Bidgoli

_____

Co-Chairperson, Dr. Michael H. Taylor

Date Approved: December 13, 2016

ABSTRACT

South-central Kansas, although historically stable, has experienced an increase in seismic activity since 2013. The correlation with brine disposal operations has renewed interest in the role of fluids in fault reactivation, specifically in the crystalline basement, where the majority of events have occurred. This study focuses on determining the suitability of CO_2 and brine injection into a Cambro-Ordovician reservoir (Arbuckle Group) for long-term storage and a shallower Mississippian reservoir for enhanced oil recovery (EOR) in Wellington Field, Sumner County, Kansas. Our approach for determining the potential for injection-induced seismicity has been to (1) map subsurface faults and estimate in-situ stresses, (2) perform slip and dilation tendency analysis to identify optimally oriented faults relative to the estimated stress field, and (3) determine the pressure changes required to induce slip, both at reservoir depth and basement depth. Through the use of 3D seismic reflection data, 12-near vertical faults were identified with fault planes striking between 325° to 049° and the majority oriented NNE, consistent with nodal planes from moment tensor solutions from recent earthquakes in Kansas and Oklahoma. Fault lengths range from 210 to 4,450+ m and vertical separations range from 12-33 m. The majority of faults cut through both reservoirs, with a number that clearly cut the top basement reflector. Drilling-induced tensile fractures (N=40) identified from image logs and inversion of moment tensor solutions (N=70) are consistent with the maximum horizontal stress (SHmax) oriented ~EW. Stress magnitudes were estimated using step rate tests (Shmin = 18.4 MPa), density logs (Sv = 36.6 MPa), and calculations from wells with drilling induced tensile fractures (SHmax = 31.3-45.9 MPa) at the gauge depth of 1,484m. Slip and dilation tendency analysis indicates that faults striking <020° are stable under reservoir conditions, whereas faults striking 020°-049° may have a moderate to high risk for reactivation with increasing pore fluid pressure. These faults

would require a pore fluid pressure increase of at least 1.1 MPa to 7.6 MPa at 1,117 m (Mississippian) and 1.31 MPa to 9.8 MPa at 1,484 m (Arbuckle) to reach failure. Given the proposed injection volume, it is unlikely that faults will be reactivated at reservoir depths. However, at basement depths, high rate injection operations could reach pressures beyond the critical threshold for slip, as demonstrated by the large number of injection induced earthquakes west of the study area.

ACKNOWLEDGEMENTS

This research was supported by the Kansas Geological Survey at the University of Kansas under grants funded by the U.S. Department of Energy (DOE) National Energy Technology Laboratory (NETL) and cost-sharing partners.

I would like to acknowledge several people who were kind enough to provide their time, expertise, and data that were critical for furthering my research in Wellington Field. I am grateful for Eugene Holubnyak and Mina FazelAlavi for providing me with data that directly affected my analysis, and further providing their time to explain the process and significance of their work. I would also like to thank Jason Rush for his assistance with navigating Petrel™ software. I would not have been able to do my analysis without the input of Alan Morris and his software, 3DStress. Thank you for taking the time to answer all of my questions, and keeping me up to date on new features in the program. Finally, I would like to thank Lynn Watney who was always willing to sit down and discuss my work and answer any questions that I had, and always with a positive and encouraging attitude.

Finally, I would like to express my respect and thanks to my advisors Tandis Bidgoli and Michael Taylor. I have learned so much from them both over these past 2+ years, and owe them a great bit of gratitude for their hard work and support of me and my research. I would also like to acknowledge my committee member Leigh Stearns who was always available to provide her input and honest opinion, and for processing many months of cGPS data for me.

TABLE OF CONTENTS

LIST OF FIGURES

LIST OF TABLES

INTRODUCTION

Injection-induced earthquakes are a growing concern near underground injection control (UIC) class II wells across the central and eastern U.S. (CEUS). These wells dispose of fluid waste, co-produced with oil and gas, reinjecting it into subsurface reservoirs for long-term storage and for secondary oil and gas recovery. Since 2009, the number and rate of earthquakes near such injection operations has sharply increased, including areas in Kansas (e.g., Buchanan, 2015), Texas (e.g., Frohlich, 2012), Arkansas (e.g., Horton, 2012), Ohio (e.g., Kim, 2013), New Mexico (e.g., Rubinstein et al., 2014), and Oklahoma (e.g., Keranen et al., 2014). Although the vast majority of class II wells across the country operate without incident (e.g., Elsworth, 2013; Weingarten et al., 2015), the recent surge in seismicity has challenged assumptions about the safety and efficacy of underground fluid injection (brine or CO_2; e.g., Zoback and Gorelick, 2012). At the same time, booming development of unconventional (i.e., low permeability) resource plays that typically have high water to oil ratios and increased regulations on the emissions of greenhouse gases (CO_2), means that the need for additional injection wells is growing, as are the operational demands on existing wells.

The primary risk for induced seismicity has been injection of wastewater into deep strata or basement formations near pre-existing faults (e.g. Evans, 1966; Healy et al., 1968; Raleigh et al., 1976) (Zoback and Gorelick, 2012; Elsworth, 2013). Typically, faults will not reactivate as long as the applied shear stress is less than the stress of the contact. The failure condition is expressed by the equation, $\tau_{crit} = \mu(\sigma_n - P) + \tau_o$ where τ_{crit} is the critical shear stress, μ is the coefficient of friction (0.6 to 1.0), σ_n is the effective normal stress, P is the pore pressure, and τ_o is the cohesive strength. This equation is then modified for Byerlee material (cohesionless fault) in which there is no shear strength ($\tau_o = 0$) (Bylerlee, 1978). Failure can be reached by

increasing the shear stress, reducing the normal stress, and/or elevating the pore fluid pressure. The likelihood of induced events is influenced by (1) the magnitude of the pore fluid pressure perturbation, (2) the spatial extent of the pore fluid pressure change, (3) ambient stress condition close to failure condition and (4) faults that are optimally oriented for failure (Elsworth, 2013). The rate of injection (e.g., Weingarten et al., 2015) and the presence of a hydraulic connection to deeper faults (e.g., Townend and Zoback, 2000) can also influence the likelihood for induced events.

South-central Kansas, the location of our study area, is part of the stable midcontinent where historical seismicity has been low (Figure 1). Low strain rates paired with ideal reservoir conditions including depth (1,270 m), thickness (305 m), confinement, permeability (up to 1,500 md), and pore fluid pressures (14.6 MPa) have made the Arbuckle reservoir ideal for brine disposal for decades, and demonstrates its potential for CO_2 disposal. However, since 2012, concentrated and high rate brine disposal operations have led to increased seismicity, including, in 2014 and 2015, earthquakes of M4.9 in western Sumner County, and a M4.3 and M4.1 in Harper County, Kansas. There have also been over 100 M3.0+ earthquakes in Harper and Sumner County since 2012 (Figure 1 and 2) (from ANSS, 2016). The majority of these events occur within the crystalline basement, at depths of 3-7 km, well below the primary injection interval, suggesting a hydraulic connection with basement faults (from ANSS, 2016). A major challenge for stakeholders in Kansas and other parts of the CEUS is that subsurface faults and stresses are not well known, making it difficult to properly site new disposal wells or make informed decisions regarding existing disposal wells. Industry 2D and 3D seismic reflection data sets that could aid in identifying subsurface faults are generally lacking and well log data that provide constraints on the in-situ stresses have not been rigorously evaluated. Such detailed

characterization of subsurface faults and in-situ stresses is critical for accurate assessments for the potential of induced seismic hazards.

This study is focused on evaluating the potential for induced seismicity associated with fluid injection into two subsurface reservoirs as part of a planned small-scale CO_2 injection project in Wellington Field, Sumner, County, Kansas (Figure 1). Target injection depths are within the Mississippian series (1,116–1,129 m) for the purpose of EOR (KGS 1-32) and the Cambro-Ordovician Arbuckle group (1,496-1,539 m) for the purpose of long-term CO_2 sequestration (KGS 1-28), both of which are heterogeneous deep saline limestone-dolomite reservoirs (Walters, 1958; Goebel, 1966; Zeller, 1968). The combination of 3D seismic reflection data, image logs, well log, and test data (e.g., step rate tests) enable a more robust analysis of potential faults and reservoir conditions, not typically available at injection sites across the U.S. midcontinent. Such analyses can provide a better understanding of injection conditions that lead to induced seismicity, including whether the proposed volume of CO_2 (40,000 tonnes) poses any seismic hazard.

This paper focuses on determining the likelihood of slip for faults located in the subsurface at Wellington field. The suitability of injection at Wellington field is evaluated for both the proposed CO_2 injection volume (40,000 tonnes) and for commercial-scale fluid injection of brine or CO_2. Through 3D seismic mapping of stratigraphic horizons and faults, along with a detailed stress field analysis, we show that under current reservoir conditions, faults appear to be stable and require significant pore fluid pressure changes to reactivate (1.1-9.7 MPa), much higher than the estimated pressure change for the proposed injection volumes (0.4-<0.15 MPa). However, the occurrence of nearby induced events below the injection interval, within the Precambrian basement, suggests the presence of large, conductive, and critically stressed faults

that may reactivate in response to small pore fluid pressure change. Therefore, although our results suggest a low likelihood for injection-induced fault reactivation associated with pilot-scale injection, we show that reservoir-based assessments may be inadequate for proper hazard characterization for faults within the Precambrian crystalline basement under commercial-scale injection.

STUDY AREA

Wellington Field, located in north-central Sumner County, encompasses approximately 20.7 km^2 of south-central Kansas (Figure 1). The oil field was discovered in 1929 and has produced over 20 million barrels of oil over its history, through nearly 300 wells and successful waterflooding operations (KGS, 2016). Current oil production has slowed to 55 producing wells (KGS, 2016). Production in the field and recent CO_2-EOR efforts are focused on Mississippian reservoirs, while the underlying Arbuckle Group saline aquifer system is routinely used in the region for wastewater (UIC class II) and hazardous waste (UIC class I) disposal, and is the proposed target for long-term storage of CO_2.

Wellington Field resides in the southern part of the Sedgewick Basin, which is bounded by the Nemaha Ridge-Humboldt fault zone (NRHF) to the east and Pratt anticline and Central Kansas Uplift (CKU) to the west. The ~50 km wide, NNE-trending NRHF extends 500 km, from Nebraska to Oklahoma and borders the Forest City Basin to the east and the Salina Basin to the west (Lugn, 1935; Lee and Merriam, 1954; Steeples et al., 1979; Stander, 1989). The NRHF is one of several regional structures within the U.S. midcontinent that has been identified from subsurface data, including potential field anomalies (e.g., Kruger, 1997), limited seismic reflection data (e.g., Steeples, 1979; Stander, 1989), and well log data (e.g., McBee, 2003). There are a number of faults associated with the NRHF system, including the Humboldt fault, a strike-

slip fault located on the eastern flank of the NRHF. Earthquake epicenters are clustered throughout the NRHF (Merriam, 1956; Steeples, 1996; Gerhard, 2004).

The NRHF system strikes sub-parallel to the late Precambrian Midcontinent Rift System (MRS), which is approximately 40 km to the west. The NRHF and MRS appear to have similar tectonic origin, as evidenced by the geometry of the NRHF and by lower Paleozoic erosion and sedimentation that appears to be affected by NRHF movement (Gerhard, 2004). The MRS occurs from central Kansas to the northeast through Nebraska, Iowa, and Minnesota, terminating near the Lake Superior region. Rifting stopped after spreading only 50-80 km (Woelk and Hinze, 1995; Steeples, 1996). The MRS is recognized by a positive central high and flanking minima on both gravity and magnetic maps, which suggests a horst and graben geometry (Thiel, 1956; Lyons, 1959; Hinze, 1963; King and Zietz, 1971; Oray et al., 1973; Hinze et al., 1982).

To the west of the study area is the Central Kansas Uplift, a regional NW-trending structural feature that occupies much of the central part of the state (Koester, 1935; Merriam, 1963). It is an important feature for petroleum exploration and production, and was originally revealed by drilling operations. The structure developed through several periods of warping and faulting as early as pre-Cambrian time, with folding occurring primarily in the Pennsylvanian and post-Cretaceous time (Koester, 1935). Along the flanks and crests of the CKU are secondary structures, including prominent anticlines and strike-slip and normal faults that are generally stable, but have experienced recent seismicity (Merriam, 1963). Also to the west of the study area is the Pratt anticline, a broad, south plunging fold that initiated due to deformation in the early Paleozoic and reactivated in pre-Desmoinesian post-Mississippian time (Merriam, 1963).

The NRHF, MRS, and CKU are continental-scale features that are associated with myriad of smaller-scale faults developed within the shallower Paleozoic stratigraphy. Baars and Watney (1991) show that for many of the major stratigraphic packages in Kansas (e.g., Arbuckle Group, Mississippian, Lansing-Kansas City groups), erosion, facies patterns, and diagenesis are all strongly influenced by tectonics, suggesting that reactivation of basement faults occurred many times prior to well documented Pennsylvanian exhumation and erosion of the NRHF and CKU. Episodic reactivation of basement structures is also consistent with the distribution of historic and instrumentally recorded earthquakes across the state, which are generally aligned with these known structures.

Injection reservoirs

The Mississippian Series, which serves as the reservoir for EOR, is observed throughout the state including Harper and Sumner counties at depths of ~1,036 m (Figure 3) (Evans and Newell, 2013). The Mississippian series consists of interlayers of limestone and chert that can be divided into two lithological sequences that consist of: (1) older, shallow marine limestone, chert, and cherty limestones, with occasional interbeds of shale, and (2) younger marine and non-marine shales and sandstones with minor limestones (Newell et al., 1987; Watney et al., 2002; Evans and Newell, 2013).

The Upper Mississippian Series consists of limestone and dolomite with interbedded sandstone and shale, as well as some deposits of chert (Goebel, 1966; Goebel, 1968; Zeller, 1968). Descriptions from core at KGS 1-32 reveal the lithology of the Upper Mississippian Series as a moderately argillaceous, fine peloidal limestone to micritic lime mudstone with massive chert (Scheffer, 2012). The series comprises the Meramecian and overlying Chesterian stages (Goebel, 1966; Goebel, 1968; Zeller, 1968). The Chesterian stage, bounded at the top by

an unconformity, contains the oil-producing units and is the proposed target depth for CO_2 injection for EOR.

The Lower Mississippian Series consists of shale, limestone, dolomite, and chert with cherty dolomite dominating the sequence (Lee, 1956; Goebel, 1966; Goebel, 1968; Zeller, 1968). Core measurements at KGS 1-32 demonstrate that the Lower Mississippian contains tight (low porosity and permeability) and uniform lithology, and may serve as a suitable seal for the Arbuckle aquifer. Core porosities range between 0.58% to 7.16%, with permeabilities as low as 50md. The most prominent seals within the series are argillaceous dolomitic siltstone (Scheffer, 2012).

The Cambro-Ordovician Arbuckle Group serves as our reservoir for carbon capture and storage (CCS), and is also present across most of the state (Figure 3). The Arbuckle Group consists primarily of dolomitic limestone interbedded with shales (Merriam, 1963; Cole, 1975; Franseen, 2000). It unconformably overlies Precambrian granitic basement and is unconformably overlain by middle Ordovician sandstone and shale. Lithofacies distributions within the Arbuckle result in a range of porosities (1%-30%) and permeabilities (0.005-1500 md). Karst features are also abundant in the Arbuckle Group and can result in complex porosity and permeability relationships (Franseen et al., 2003; Franseen, et al., 2004).

The Arbuckle Group consists of three different formations: the Jefferson City-Cotter dolomite (JCC), Roubidoux Formation, and Gasconade Dolomite-Gunter Sandstone. The JCC Dolomite is described as consisting primarily of coarsely granular, cherty dolomite with the upper part of the interval being oolitic chert and transitioning at the base to tripolitic chert (Keroher and Kirby, 1948; Zeller, 1968). Descriptions provided by the KGS 1-32 core indicate the JCC is approximately 150 m thick, consisting of medium-grained packstones to grainstones

with interbeds of argillaceous dolomite, as well as micritic dolomite in the lower portion of the formation (Scheffer, 2012). The Roubidoux Formation is a sandy dolomite and fine-grained sandstone (Keroher and Kirby, 1948; Goebel, 1968; Zeller, 1968). Core at KGS 1-32 determined a thickness of 79 m (Scheffer, 2012). The Gasconade Dolomite is a cherty, coarsely granular dolomite with a sandy dolomite member (Gunter sandstone) near its base (Keroher and Kirby, 1948). Core at KGS 1-32 reveal that the Gasconade is 77 m thick, resting unconformably on the Precambrian basement (Scheffer, 2012). The proposed injection depth for CO_2-CCS lies at the base of the Gasconade Dolomite (1,496-1,539 m). The Simpson group, which directly overlies the Arbuckle Group, contains 30 m of limestone and sandstone that is considered to be part of the CCS reservoir (Figure 3).

The Chattanooga shale overlies the Simpson group and serves as the primary seal for CCS in the Arbuckle Group (Figure 3). The Chattanooga Shale is dolomitic and silty, and ranges in thickness regionally from 1 to 50 m (Lee, 1940; Goebel, 1968; Zeller, 1968). Well logs at KGS 1-28 indicate a thickness of 15 m, however, the thickness at KGS 1-32 was only 15 cm due to erosion (Lee et al., 1948).

Both the Arbuckle Group and Mississippian Series reservoirs have pore fluid pressures below hydrostatic (Bradley, 1975; Puckette and Al Shaieb, 2003; Sorenson, 2005; Nelson and Gianoutsos, 2011). The abnormally low reservoir pressure is a consequence of the departure between surface elevations and hydraulic head, which is the result of a major hydrodynamic adjustment associated with post-Laramide uplift, erosion, and formation water discharge (Sorenson, 2005; Nelson and Gianoutsos, 2011). Oil and gas production from the Mississippian has resulted in further reduction of pore fluid pressures down to 6.2 MPa. These subnormal

reservoir pressures attest to the adequacy and regional extent of seals, and make these vertically confined reservoirs ideal for fluid injection.

METHODS

Fault mapping and characterization

To determine reservoir fault geometries, we utilized 3D seismic-reflection data across the study area, including Wellington field to the south and Anson Bates field to the north. The data volume has an area of 41.3 km^2, a depth of 1.89 km, and contains 541 in-lines, and 251 cross-lines. Acquisition and processing of the seismic reflection data was optimized for imaging the Arbuckle Group and Mississippian Series; therefore, data quality and resolution are diminished, in some instances, below the Arbuckle.

Faults and stratigraphic horizons were mapped using standard seismic interpretation procedures in Petrel™. Stratigraphic horizons were tied to the seismic reflection data using 210 wells and top reflectors for the basement, Arbuckle Group, Mississippian Series, Kansas City Limestone, and Topeka Limestone were mapped. Faults were mapped in vertical seismic reflection profiles by identifying offsets or discontinuities in these and other arbitrary horizons. Depth slices were also useful in identifying faults and determining the lateral extent of faults by locating abrupt breaks in reflection amplitude (Bahoric and Farmer, 1995). To increase confidence in our fault interpretations, we utilized seismic attributes analysis by evaluating coherency, which highlights trace-to-trace variability and changes in acoustic impedance (Bahoric and Farmer, 1995). We evaluated the established faults using several criteria, including (1) fault geometry, (2) fault length to width and length to displacement ratios (e.g., Wells and Coppersmith, 1994; Hanks and Bakun, 2008), (3) continuity between seismic profiles, and (4) consistency with other known geological structures (e.g., Lugn, 1935; Lee and Merriam, 1954;

Steeples et al., 1979; Stander, 1989). Fault geometry was measured in Petrel™ for strike, dip, length, width, and vertical separation (Table 1). Faults and stratigraphic horizons were then modeled as 3D surfaces to visualize spatial relationships and to identify any inconsistent interpretations.

Stress orientations

Assuming one of the principle stresses is the vertical stress (Sv), the orientation of the maximum and minimum horizontal stresses (SHmax and Shmin, respectively) can be determined by analyzing image and other types of well logs for drilling induced tensile fractures (Aadnoy, 1990; Moos and Zoback, 1990; Wiprut and Zoback, 2000) and borehole breakouts (Figure 4) (Bell and Gough, 1979; Zoback et al., 1985, Zoback et al., 2003). In an open hole, circumferential stresses concentrate around the wellbore walls and are variable with azimuth. The circumferential stress is lowest at the azimuth of the SHmax and highest at the azimuth of the Shmin. Drilling induced tensile fractures initiate parallel to the direction of SHmax when the wellbore wall goes into tension, which is often the case when there are large differences between Shmin and SHmax (Aadnoy, 1990; Moos and Zoback, 1990). Drilling induced tensile fractures appear on image logs as narrow, well-defined conductive features separated by 180 degrees (Figure 4) (Tingay et al., 2008). In contrast, borehole breakouts occur parallel to Shmin, when the circumferential stress exceeds the compressive strength of the rock at the wellbore (Zoback et al., 1985; Bell, 1990, Tingay et al., 2008). Borehole breakouts appear on image logs as broad, parallel, often poorly resolved conductive features separated by 180 degrees (Figure 4) (Tingay et al., 2008).

Across south-central Kansas, 6 wells were evaluated and 4 were identified as having drilling induced tensile fractures (Figure 1). No borehole breakouts were identified. Individual

fractures varied in orientation from top to bottom, with up to 010° of deviation. Measurements were taken near the top and the base of each individual fracture. Exact measurement locations varied and were dependent on the best representation as determined by the interpreter. All of the measurements were then averaged to estimate the orientation of SHmax. A quality ranking system established by Zoback and Zoback (1991) was used to better characterize the accuracy of measurements taken from each well (Table 2). The rankings were based on the quality of the wellbore fractures and breakouts. Generally, estimations were considered of higher quality (A rating) when there were larger numbers of distinct measurements, larger sizes of the fractures or breakouts, and smaller deviations between distinct measurements.

Earthquake moment tensor solutions are also a widely used present-day stress indicator (e.g., McKenzie, 1969; Gephart and Forsyth, 1984; Michael, 1984, 1987; Yih-Hsiung, 1989; Zoback, et al., 1989). Although the azimuth and plunge of the principal axes of moment tensor solutions are not directly equivalent to the principal stress axes, one can use them as an indirect approximation of the stress field. The maximum principal stress direction, for example, will lie with the dilational quadrant of a moment tensor solution (e.g., McKenzie, 1969). A number of computer-based inversion processes have been developed with consistent results, suggesting that inversion of moment tensor solutions is a reasonable estimator for stress orientations (Angelier, 1979; Ellsworth and Zhonghuai, 1980; Ellsworth, 1982; Gephart and Forsyth, 1982; Michael, 1984). The software package used in this study, STRESSInverse, was modeled after the method demonstrated by Michael (1984, 1987) (Vavrycuk, 2014). By this method, using the tangential traction on a number of planes in a region, and by assuming that the slip events are independent and represent the same stress tensor, it is then possible to determine the stress field. The end

result is a single uniform stress tensor that most likely influenced the faulting events (Michael, 1984, 1987; Vavrycuk, 2014).

For this study, we inverted 70 moment tensor solutions, from recent injection-induced earthquakes in south-central Kansas and north-central Oklahoma, for principle stress directions (Figure 1; Table 3). Earthquake moment tensor solutions were recorded by the NEIC (National Earthquake Information Center) for earthquakes of moment magnitude 3.0 and higher from January 1, 2012 through April 28, 2016. Input parameters for the inversion are strike, dip, and rake associated with one of the nodal planes. The nodal plane selected for inversion was the plane consistent with both the fault plane orientations observed in the study area and the known structures in the region, primarily with nodal planes striking ~NNE. Although it is not necessary to use the nodal plane that represents the actual fault plane, doing so will result in better confidence regions and better allows the algorithm to manipulate the data set to find an acceptable uniform stress field (Michael, 1987). Both strike-slip (SS) and normal-slip (NS) moment tensor solutions were available. Because the orientation of σ_1 is different for SS and NS stress environments, the inversion was done separately for SS and NS moment tensors to avoid conflicting inputs and to prevent inaccurate results. We note that SS and NS moment tensors occur in close proximity to one another, suggesting that the stress magnitude of both principal axes is similar as well. Stress inversion of the moment tensor solutions had up to 2000 iterations using a bootstrap resampling method to ensure a higher confidence in the result. Bootstrap resampling randomly selects moment tensor data for the given sample size, in our case N=39 (SS) and N=31 (NS), with some moment tensors repeated, while others are absent. By repeating this process 2000 times, the true variation in the data is revealed, with an end result that more closely resembles the best fit stress field (Michael, 1987).

Stress magnitudes

The vertical stress (Sv) was calculated from density logs in 11 wells in south central Kansas including KGS 1-28 and KGS 1-32 (Figure 1). The overburden stress is calculated by a depth integration of density using:

$$Sv = \int_0^z \rho(z) g dz \approx \bar{\rho} g z$$

where $\rho(z)$ is the density as a function of depth, g is the gravitational acceleration, and $\bar{\rho}$ is mean overburden density (Zoback et al, 2003). The calculation assumes that hydrostatic pore pressure for fresh water increases at a rate of 9.8 MPa/km (0.43 psi/ft) (Zoback et al., 2003).

To ensure accuracy, only wells where density logs reached the base of the Arbuckle, or deeper, were used. Overburden estimates at depths beyond the measured data were calculated by using a uniform density of 2.75 g/cm^3. This value was derived from accepted basement rock density averages and is in agreement with shallow basement density measurements taken from density logs in south central Kansas (Smithson, 1971).

In order to estimate the magnitude of Shmin, step rate test data from KGS 1-32 was analyzed at a gauge depth of 1,484 m. Both the breakdown pressure, the pressure required to initiate a fracture, and the closure pressure, the pressure required to hold a fracture open, were identified (FazelAlavi, 2016). Because the pressure needed to propagate a hydraulic fracture is controlled by the magnitude of the least principal stress, the closure pressure is the best approximation of the magnitude of Shmin (Zoback et al., 2003; Nelson et al., 2007). Another step rate test in Harper County (Yeti 1-15 well in the Wharton South Field) was analyzed and a breakdown pressure was identified, but no closure pressure was interpreted from the data.

Calculation of SHmax was completed through equations (1) and (2), which are considered an acceptable method for estimating SHmax when drilling induced tensile fractures are present

in a borehole (Zoback et al., 2003). Equation 1 was derived from equation 3, which represents the conditions at which a tensile fracture in the wall of a vertical wellbore occurs (Zoback et al., 2003). Zoback et al. (2003) shows that it is acceptable to assume that ΔP and $\sigma^{\Delta T}$ are close to 0 by comparing results of equation 1 with estimated stress polygon values. Equation 2 is used to account for any variation in pore fluid pressure (Pp) at depth:

1) $SHmax = 3Shmin - 2Pp$

2) $SHmax = 3Shmin - Pp$

3) $3Shmin - SHmax - 2\,Pp - \Delta P - \sigma^{\Delta T} = 0$

Stress magnitudes at basement depth (5.85 km) were calculated using a stress polygon (e.g., Zoback, 2003) for a coefficient of friction (μ) of 0.6 (Byerlee, 1978). Boundaries of the stress polygon represent the failure limits for the given stress values for different stress states (NS, SS, or RS). Boundaries were defined by the following equations (Zoback et al., 1987; Moos and Zoback, 1990):

4) $F(\mu) = [sqrt(\mu^2 + 1) + \mu]^2$

5) $SHmax = F(\mu)(Sv - Pp) + Pp$

6) $SHmin = (Sv - Pp)/f(\mu) + Pp$

Slip and dilation tendency analysis

To determine the likelihood of fault reactivation, we used the observed fault geometry combined with the estimated stress state to compute the slip and dilation tendency (Morris et al., 1996; Worum et al., 2004). Slip tendency (T_S) is the ratio of shear stress (τ) to normal stress (σ_n) acting on a fault. For slip to occur on a cohesionless fault (i.e., reactivation of a Byerlee material), the resolved shear stress must be equal to or greater than the frictional resistance to sliding, governed by the coefficient of friction (Morris et al., 1996). In other words, if the slip

tendency value exceeds the value of the coefficient of friction, slip will occur. Dilation tendency (T_d) is the likelihood for a fault or fracture to dilate based on the three-dimensional stress conditions. Dilation tendency values range from 0 – 1 with higher values indicating a more optimal orientation for dilation. Slip and dilation tendency are defined by the following equations:

7) $T_s = \tau / \sigma_n$

8) $T_d = (\sigma_1 - \sigma_n)/(\sigma_1 - \sigma_3)$

Slip and dilation tendency analyses were completed on the modeled faults using 3DStress® (Morris et al., 1996; e.g., Worum et al., 2004). Along with the fault models, the orientation and magnitude for σ_1, σ_2, and σ_3 were input into 3DStress®. Slip and dilation tendency was calculated for individual fault planes and projected onto the fault surfaces. Slip and dilation tendency for both SS and NS stress states in the Arbuckle and Mississippian was calculated based on the lowest and highest values of SHmax (eq. 1 and 2) and using the average estimated orientation of SHmax (075°). At basement depths, the magnitude of SHmax is based on frictional failure equilibrium assuming Andersonian faulting (Anderson, 1951), estimated from the boundaries of a stress polygon (Moos and Zoback, 1990; Zoback et al., 2003). The stress polygon reveals a possible range of SHmax and Shmin values consistent with a SS stress state. Therefore, the analysis was completed using intermediate magnitudes for both, and then compared to results using the highest and lowest possible magnitudes for both. For a NS stress state, an intermediate value for SHmax was used. Slip and dilation tendency estimates were completed using the measured stress state at Mississippian (1.12 km) and Arbuckle (1.48 km) depths, as well as the estimated stress state at a basement depth of 5.85 km, the average depth of NEIC reported induced events in Kansas.

In addition to evaluating the likelihood of failure using the above approach, we evaluated the fault geometries in Mohr space to evaluate the sensitivity to failure due to changes in pore fluid pressure. By forward modeling the pore fluid pressures required for failure, a critical pressure threshold was determined for each fault. For our study, we assume a μ of 0.6 and compare this with a more conservative estimate using 0.5 (Byerlee, 1978). Additionally, we evaluated pore fluid pressure changes for SS and NS stress states at depths in the Mississippian, Arbuckle, and basement. We also conducted sensitivity analyses to evaluate the effects of stress orientation and magnitude to better quantify uncertainties in slip tendency calculations.

RESULTS

Fault Geometry

Within the 3D dataset for the Wellington and Anson Bates Fields, we identified 12 – mostly vertical faults, striking between 325° to 049°, with the majority of the faults striking NNE (Figure 5 and 6) (Table 1). By comparison, naturally occurring conductive fractures identified in image logs from wells KGS 1-28 (N = 12) and KGS 1-32 (N = 12) have similar orientations, with the majority ranging from 20°-40° and 10°-20°, respectively (Figure 7). The NNE striking faults are consistent with the NNE-trending Nemaha uplift, Humboldt fault zone, and Midcontinent Rift system, as well as with nodal planes from moment tensor solutions for recent earthquakes in south-central Kansas and northern Oklahoma (Figure 1). The majority of the faults cut both the Mississippian and Arbuckle. Although the data quality is diminished near the base of the Arbuckle, several faults were observed cutting the top of the crystalline basement as well (faults 1, 2, and 3). Only one fault (9) fails to cut the Arbuckle and is contained within the Mississippian formation.

Faults were measured with lengths ranging from 210-4,450+ m, widths between 100-1,000+ m, and vertical separation between 12-33 m (Table 1). At least three of the faults (1, 2, and 3) extend beyond the boundaries of the 3D seismic volume and vertically below the base of the Arbuckle (Figure 6), suggesting that they are likely longer and deeper than our measurements, which should be considered when evaluating the seismic hazard associated with these structures. The largest of the mapped faults is at least 4,450 m in length, at least 914 m in width and has 33 m of vertical separation. Fault length area-scaling relationships suggests the structure has the potential for a M5.8+ earthquake, although it is unlikely that the entire fault would reactivate during a single event (Wells and Coppersmith, 1994; Hanks and Bakun, 2008). However, this earthquake potential is not entirely accurate because the full extent of the fault is unknown.

Stress orientations and magnitudes

The orientation of SHmax was estimated by measuring the orientation of 40 drilling induced tensile fractures from wells KGS 1-28 (N=5), KGS 1-32 (N=5), McGrath 1-16 (N=15), and Spriggs 1-34 (N=15) (Figure 1). The majority of induced fractures were centerline fractures (N=32), however petal fractures were also recorded (N=8). Fractures range in width between 200 m and 1 m, with the majority below 30 m (Table 2). Based on the criteria established by Zoback and Zoback (1991), wells KGS 1-28, KGS 1-32, McGrath 1-16 are graded C, and well Spriggs 1-34 is graded B (Table 2). The relatively low grades are based on small sample size and widths of the fractures. Fracture orientations range from 055° to 087°, with an average of 077° and standard deviation of 007° (Figure 8). Inversion of SS (N=39) and NS (N=31) moment tensor solutions provides a best-fit stress state with an average SHmax oriented ~075°. There does not appear to be any local trends in nodal plane orientation or sense of slip in the sample

area, suggesting that the stress state is consistent across the study area (Figure 1). The estimates from SS (SHmax=80°) and NS (SHmax=70°) moment tensors were processed separately with 2,000 repetitions each to increase confidence to around 95% (Michael, 1987) (Figure 9). These results are consistent with detailed stress analyses in Oklahoma which also suggest an SHmax orientated ENE for both SS and NS moment tensor solutions (Dart, 1990; Holland, 2013; Alt and Zoback, 2015).

Stress magnitudes for Sv (36.6 MPa), Shmin (18.4 MPa), and SHmax (31.3-45.9 MPa) were estimated at a depth of 1,484 m within the Arbuckle formation. Stress gradients (Sv = 24 MPa/km; Shmin = 12.4 MPa/km; SHmax = 21-31 MPa/km), shown in Figure 10, are based on the calculated stress magnitudes at gauge depth. Stress magnitudes are calculated at Mississippian depth (1,120 m) for Sv (27 MPa), Shmin (14 Mpa), and SHmax (23-34 MPa). The range in SHmax overlaps values of Sv, consistent with the observed SS or NS moment tensor solutions. The pore fluid pressure calculated at 1,484 m is 14.5 MPa using a freshwater hydrostatic gradient (9.8 MPa/km).

At basement depth (5.85 km), the estimated Sv is 155.3 MPa and is used to construct a stress polygon for a coefficient of friction of 0.6 (Figure 11). The boundaries of the stress polygon indicate the possible range of SHmax and Shmin magnitudes at failure. For a SS stress state, an intermediate estimate using a mid-range value for SHmax (201 MPa) and Shmin (103 MPa) is used for slip tendency analysis. Results were then compared to the highest (SHmax = 363 MPa; Shmin = 155 MPa) and lowest (SHmax = 155 MPa; Shmin = 89 MPa) possible stress value combinations for a SS stress state. For a NS stress state, slip tendency analysis uses stress values at failure equilibrium with an intermediate value for SHmax (138 MPa).

Potential for fault reactivation

Results from the slip tendency analysis for the observed faults in the Mississippian reservoir are shown in figures 12 and 13 for an SHmax oriented 075°. We estimate the stress state Sv (27 MPa), Shmin (14 MPa), and SHmax (23-34 MPa) using the stress gradients calculated at the injection interval (1,116 to 1,129 m). The highest and lowest values of SHmax for SS (34 MPa) and NS (23 MPa) stress states were used in the final slip tendency analysis. For a SS stress state, slip tendency values ranged from 0.46 to 0.01. By projecting fault planes into Mohr space, we estimate the critical pore fluid pressure that would promote failure. At Mississippian depth, optimally oriented faults would require an additional pore fluid pressure of 1.1 MPa (μ=0.5) to 4.13 MPa (μ=0.6) to induce favorable conditions for failure on faults in a SS stress state (SHmax = 34 MPa) (Figure 12). Based on the stress field, faults were determined to be poorly to optimally oriented for failure in a SS stress state, with the majority of faults being moderately oriented for failure. In a NS stress state (SHmax = 23 MPa), slip tendency values were less than 0.34 with a required pore fluid pressure change of 5.79 MPa (μ=0.5) to 7.6 MPa (μ=0.6) to reach failure on optimally oriented faults (Figure 13). Faults are mostly moderately to poorly oriented for failure in a NS stress state. Dilation tendency within the Mississippian is low overall, with most fault planes having dilation tendency values less than 0.3. Due to high differential stresses, slip is much more likely.

The results from the slip tendency analysis for faults in the Arbuckle reservoir are shown in figures 14 and 15 for an SHmax oriented 075°. Stress magnitudes at the Arbuckle reservoir depth of 1,484 m is calculated for Sv (36.6 MPa), Shmin (18.4 MPa) and SHmax (31.3-45.9 MPa). In a SS stress state, assuming the highest estimated value for SHmax (45.9 MPa), slip tendency reached values up to 0.47 (Figure 14). Depending on the fault zone properties, in order

for optimally oriented faults to reach failure, an increase in pore fluid pressure of 1.31 MPa (μ=0.5) to 5.37 MPa (μ=0.6) is required (Figure 14). In a NS stress state (SHmax = 31.3 MPa), slip tendency values reached up to 0.35 (Figure 15). An increase in pore fluid pressure of 7.0 MPa (μ=0.5) to 9.8 MPa (μ=0.6) is required to reach failure conditions for optimally oriented faults (Figure 15). Dilation tendency values within the Arbuckle are also low, with most fault planes having dilation tendency values less than 0.2.

Slip tendency analysis at basement depth for a SHmax oriented 075° was also conducted using a stress polygon, assuming Andersonian faults in failure equilibrium (e.g., Moos and Zoback, 1990; Zoback et al., 2003). Due to limitations of the seismic data, which prevented mapping of faults at deeper basement depths, shallow faults were projected to 5.85 km, the average depth of NEIC reported injection-induced earthquakes in south-central Kansas. Assuming a SS stress state, the slip tendency analysis demonstrates that portions of 2 faults (7 and 10) are already at failure and would slip in response to very small pore fluid pressure changes, 3 of the faults (2, 3, and 12) would slip in response to pore fluid pressure changes greater than 3.4 MPa, and the remaining 7 faults (1, 4, 5, 6, 8, 9, and 11) were unlikely to fail under the presumed stress state, requiring a change is pore fluid pressure of 13 MPa or more to reach failure (Figure 16). Furthermore, in a NS stress state, none of the faults are near failure, 5 faults (2, 3, 7, 10, and 12) would slip with a pore fluid pressure increase of 5.4 MPa or more, and the remaining 7 faults (1, 4, 5, 6, 8, 9, and 11) were more unlikely to fail, requiring a change in pore fluid pressure of 14.5 MPa or more (Figure 17).

Uncertainties associated with the stress polygon estimations indicate a possible range of SHmax and Shmin values (Figure 11). When compared to the intermediate analysis, slip tendency analysis using the highest values of SHmax (363 MPa) and Shmin (155 MPa) for a SS

stress state brings additional faults to failure, including areas of faults 1, 7, and 12, and the entirety of fault 10. Conversely, faults are more stable using lower values of SHmax (155 MPa) and Shmin (89 MPa), with only a small portion of fault 12 reaching failure conditions. Considering the occurrence of induced events to the west and south indicating a critical stress state, and the presence of both SS and NS moment tensor solutions indicating similar magnitudes for SHmax and Sv, it is likely that the intermediate estimates (Figure 16 and 17) more closely represents the actual stress state at basement depth.

DISCUSSION

Potential for fault reactivation within the Mississippian and Arbuckle

Based on the mapped fault orientations and geometries, their relationship to the estimated stress field, and the volume of CO_2 planned for injection (40,000 tonnes/well), the faults in the study area appear to be stable at reservoir depths (Mississippian; 1,116–1,129 m and Arbuckle; 1,496-1,539 m). Fault strikes range between 325° and 049°. Relative to our estimates of the stress field, an optimally oriented fault would strike between 035°-057° in a SS stress state and normal faults would strike between 066°-092° - these values are consistent with observed nodal planes from earthquake moment tensor solutions, which ranged between 000°-064° (SS) and 038°-105° (NS) (Figure 9) (ANSS, 2016). Although two of the mapped faults (7 and 10) fall within the range of optimal orientation for a SS stress regime, the majority are only moderately (2, 3, and 12) to poorly (1, 4, 5, 6, 8, 9, and 11) aligned for reactivation, as demonstrated by the slip tendency analysis, shown in figures 12-17.

Although the orientations of at least two of the mapped faults suggest risk for reactivation, further analysis reveals that even the most susceptible faults, including fault 7 which is in close proximity to the injection wells (0.25 km), would require a significant increase

in pore fluid pressure to initiate failure (Figure 12-17). Maximum pressure changes associated with the planned CO_2 injection activities at Wellington Field were determined through numerical multi-phase flow simulations for the Mississippian and Arbuckle reservoirs (Holubnyak et al., 2016). The models, which incorporate well log, 3D seismic reflection, well test data, and a host of other reservoir parameters (e.g., temperature, fluid properties, relative permeability, and capillary pressure), suggest that after 9 months of injection into the Arbuckle, the estimated pore fluid pressure change would be 0.4 MPa at the borehole and <0.15 MPa at distances of 150 m or greater from the wellbore (Holubnyak et al., 2016). By comparison, the slip tendency analysis shows that under a likely coefficient of friction (μ=0.6) and the highest risk stress state (SS), an order of magnitude increase in pore fluid pressure is required to reach failure at reservoir conditions (4.13 MPa at Mississippian; 5.37 MPa at Arbuckle). This result holds true even when a more conservative coefficient of friction (μ=0.5) is used (1.1 MPa at Mississippian; 1.31 MPa at Arbuckle). In a NS stress state, the slip tendency would be lower, requiring an even greater change in pore fluid pressure to induce failure.

Uncertainties in stress orientations and magnitudes can significantly impact the slip tendency analysis results. The most significant uncertainties are associated with the magnitudes of the horizontal stresses. Shmin is only constrained by 3 recorded pressures, all within the Arbuckle. At gauge depth (1,484 m), sensitivity tests suggest that a 10% reduction in the magnitude of Shmin would increase slip tendency by 12% (from 0.47 to 0.53) for a SS stress state, and 16% (from 0.35 to 0.41) for a NS stress state (Figure 18). Uncertainties in these values also affect SHmax, which is reliant on accurate estimates for Shmin. Similarly, the orientation of SHmax, which has a range of potential values, also introduces some uncertainty into the analysis (Figure 8 and 9). For example, a more northerly azimuth of SHmax, assuming a SS stress state,

would result in more fault planes moving into favorable orientations. Conversely, a more easterly azimuth of SHmax (081°), removes any faults from optimal orientation.

Based on the slip tendency analysis and associated uncertainties, it seems reasonable to conclude that the mass of CO_2 planned for injection is unlikely to reactivate the observed faults at reservoir conditions. The suitability of the Arbuckle and Mississippian for fluid injection is due in part to the naturally underpressured nature of the reservoirs. For the Mississippian, underpressured conditions are further enhanced by pressure depletion due to oil production, which allow for larger volumes of fluid to be injected to achieve original reservoir conditions (e.g., Bachu, 2000; Puckette and Al-Shaieb, 2003; Keranen, 2013). Furthermore, the Mississippian is currently undergoing repressurization. Injection volumes have surpassed 20,000 tonnes of CO_2 at a rate of 100-150 tonnes/day, with pore fluid pressures at near hydrostatic (11 MPa) (Holubnyak et al., 2016). Currently, there is no occurrence of induced seismicity in response to repressurization of the reservoir.

Potential for fault reactivation within Precambrian basement

Our analysis shows there is a low likelihood of reactivating faults within the Mississippian and Arbuckle—a conclusion supported by earthquake hypocenters in the region, the vast majority of which are located at 3-7 km depth, well below these reservoirs. Thus, the primary concern for the study area is reactivating basement faults. One of the most significant findings in this study is the identification of faults cutting the Arbuckle and Precambrian basement. These faults may provide hydraulic connections or pressure pathways between the Arbuckle and basement (e.g., Zhang et al., 2013). Image log analysis from wells KGS 1-28 and KGS 1-32 reveal a number of natural conductive fractures, some of which reach depths of at least 1,600 m, well into the basement rock. Orientations of these natural open fractures vary,

with the majority striking between 010° and 040°, consistent with the mapped fault orientations (Table 1; figure 7). Conductive faults paired with the lack of a seal between the Arbuckle and basement are concerning, as both are reported to have significant effect on the occurrence of induced seismicity in basement rock (Barton et al., 1995; Morris et al., 2011; Zhang et al., 2013). Elevated pore fluid pressures could propagate downward along distributed fracture networks into the Precambrian crystalline basement, suggesting that slip tendency analysis at reservoir conditions may not be adequate for characterizing the risk of induced seismicity associated with fluid injection.

If the faults at basement depth are critically stressed and in failure equilibrium, as suggested by this study and others (e.g., Towend and Zoback, 2000; Zoback and Gorelick, 2012), it is possible that even small pore fluid pressure changes (0.01 to 0.1 MPa) could induce failure (Reasenberg and Simpson, 1992; Stein, 1999; Seeber and Armbruster, 2000; Zoback and Gorelick, 2012). For example, the critical threshold for failure associated with the injection induced earthquake swarm in Jones, Oklahoma, was reported by Keranen (2013, 2014) to be 0.07 MPa. The results of our basement analysis show that several of the mapped faults, when projected to basement depth, would be in failure equilibrium, likely to fail in response to very small pore fluid pressure changes. However, when considering the earthquake potential of faults in our study area, it is important to note that only small portions of these faults would be in favorable orientations. For instance, for fault 7, only around $1/10^{th}$ of the fault area is optimally oriented, and although failure could occur in these areas under minor pore fluid pressure increases, a change in pore fluid pressure of over 35 MPa would be required to reactivate the entirety of the fault. Under such a scenario, a magnitude 5.5 event could result (Wells and Coppersmith, 1994; Hanks and Bakun, 2008), but the likelihood of such an event is exceedingly

low. Small pore fluid pressure changes, although sufficient to induce slip, would likely result in smaller magnitude earthquakes. Considering only a small number of faults have portions of their planes that are well oriented, this would suggest that although induced events are likely, the occurrence of a large-scale event is not. This is significant when determining the risks associated with large-scale injection operations, including compromised seal integrity, ground water contamination, structural damage, and safety concerns.

Implications for fluid disposal and CO_2 sequestration

Thus far, our study has addressed concerns associated with pilot-scale injection of CO_2, (~40,000 tonnes; 438,000 bbls brine equivalent), with a proposed injection rate of approximately 50,000 bbls/m. In order to have a significant impact on the total volume of CO_2 or brine generated through human activity, fluid injection must operate on a massive scale (e.g., Zoback and Gorelick, 2012), and could require the implementation of a large number of high rate injection wells. Recent seismicity in the region suggests there are challenges associated with large-scale fluid disposal, particularly when high rates of injection are considered. Weingarten et al. (2015) showed that seismicity across the U.S. midcontinent over the past 7 years strongly correlates with the development of high-rate injection wells (>300,000 barrels per month) compared to other factors like cumulative injected volume (McGarr, 1976; McGarr, 2014), proximity to basement (Kim, 2013; Zhang et al., 2013), or wellhead pressure (Frohlich, 2012; Keranen et al., 2014). The correlation between high-rate injection and seismicity is consistent with the fluid disposal and earthquake histories of Harper and Sumner counties, where brine disposal in the Arbuckle Group had operated for decades without significant issue. Prior to 2012, average injection rates per well were 16,500 bbls/m, with the highest single well injection rate reaching 83,333 bbls/m in 2008 and statewide seismicity occurred at a rate of about 1-2

earthquakes per year since 1977 (Hildebrand et al., 1988; Buchanan, 2015) [1]. Between 2012 and 2014, average injection rates per well rose to 41,140 bbls/m, with the highest single well injection rate reaching 704,471 bbls/m in 2014[1]. A concomitant increase in seismicity has been observed in these counties where more than 1,000 M2.0+ events have occurred since the end of 2013, the majority of which near high-rate waste water disposal wells (Figure 2) (from ANSS, 2016) (see Buchanan, 2015).

When considering the injection of CO_2 in areas susceptible to earthquakes, the possibility of damaging seals and causing leakage into overlying strata and underground freshwater aquifers is a major concern (e.g. Streit and Hillis, 2004; Benson and Cole, 2008; Morris et al., 2010; Vilarrassa et al., 2014; Chiaramonte et al., 2015). CO_2 is less dense and more buoyant than in-situ fluids and therefore rises to the base of overlying seals. The concern is that fracture reactivation through small to moderate earthquakes may damage the integrity of the seals and allow CO_2 to migrate vertically into shallower layers, aquifers, or even escape through to the surface and release CO_2 back into the atmosphere (Zoback and Gorelick, 2012; Shipton et al., 2016). A M4.0 event, for instance, could be associated with several mm to cm of slip along a fault (Stein and Wysession, 2009; Cappa and Rutqvist, 2011), enough to create hydraulic pathways that compromise seal integrity and allow for CO_2 to escape.

The Chattanooga shale, which serves as the primary reservoir seal, is extensive across the region with thicknesses between 1 to 50 m (Lee, 1940; Goebel, 1968; Zeller, 1968). There are also a number of shallower secondary seals, which should serve well to mitigate any risk if the primary seal were to be compromised (Lee, 1940; Goebel, 1968; Zeller, 1968). Furthermore, both the Arbuckle and Mississippian reservoirs are underpressured, an indication that pressures have not equalized over geologic timescales (Sorenson, 2005; Nelson and Gianoutsos, 2011).

[1] Class II underground injection data courtesy of the Kansas Corporation Commission

This suggests that the seals have been adequate even during geologic times when faults were likely active. Therefore, there is no evidence to suggest these seals would be compromised if any induced events were to occur.

Mitigation Strategies

Although safe fluid injection into the Arbuckle is possible, the increasing demand for fluid disposal highlights the need for alternative injection sites and alternative uses of these fluids. One possibility is injection into depleted oil and gas reservoirs like the Mississippian for waterfloods, EOR, and long-term storage.

Results from this study, along with the recent CO_2 injection test at Wellington Field, suggest that the Mississippian may serve as an adequate reservoir for secondary and tertiary recovery or for disposal of brine and/or CO_2. The Mississippian has been drawn down to approximately 6.2 MPa at Wellington field due to oil and gas production, allowing it to accept larger volumes of fluid before original reservoir conditions are met (Holubnyak et al., 2016). Local repressurization operations have raised the pore fluid pressure to near hydrostatic (11 MPa) (Watney, pers. comm., 2016). Depleted oil fields such as the Mississippian, are located throughout the midcontinent. It is estimated that oil fields in Kansas alone have an estimated 750 million barrels of CO_2-EOR potential, with a net CO_2 demand of 240-370 million tons (MGA, 2012). Waterflooding operations into the Mississippian have also proved successful. For example, the neighboring Lee and Anson Bates fields in Sumner County achieved significant production increases in response to waterflood operations, which began in the early 1980's and without any associated seismicity (Bhattacharya, 2003).

Implementation of disposal or secondary and tertiary recovery methods into the Mississippian or similar reservoirs could face a number of challenges. It requires knowledge of

compatibility of the injected fluid with connate waters and the reservoir. The fluid injected could interact with reservoir rock causing a reaction that could change the porosity and/or permeability of the reservoir (Alexeev et al., 2015; Nasralla et al., 2015). Treatment of the injected fluid could also be required in order to reduce the risk of contamination, including the removal of undesirable chemicals and bacteria (Buckley et al., 1987; Brandt and Tait, 1997). Implementation also requires significantly more in terms of reservoir management and surveillance compared to the operation of a typical saltwater disposal well. The interaction between the oil and water, for instance, could potentially increase or decrease the recovery efficiency, affecting production (Melrose and Brandner, 1974; Morrow, 1990; Tang and Morrow; 1997; Agbalaka et al., 2009). Reservoir performance indicators like breakthrough times and fluid ratios must be carefully monitored, as do reservoir pressures (e.g., Baker, 1998; Grinestaff and Caffrey, 2000).

CONCLUSIONS

3D seismic data from the Wellington and Anson Bates fields reveal 12 mostly vertical faults striking ~NNE. These faults cut Paleozoic units below the top Mississippian reflector and, where image quality is good and faults can be confidently carried, also appear to cut the top of the Precambrian basement. When evaluated within the context of the known stress field, derived from image log analysis, inversion of moment tensor solutions from recent earthquakes across the region, and well test data, these faults appear to be stable at reservoir depths. Our conservative estimates (assuming SS faulting and μ=0.5) show that these faults would require significant pore fluid pressure changes to reactivate (1.1 Mpa at Mississippian; 1.3 Mpa at Arbuckle). This analysis, however, breaks down when considering the potential for seismicity within the Precambrian basement, where these features are likely conductive and critically

stressed and can reactivate with small pore fluid pressure changes, as indicated by the recent increase in seismicity in the region (Zoback and Zoback, 1980; Zoback, 1992; Towend and Zoback, 2000; Zoback et al., 2002; Zoback and Gorelick, 2012). Thus, our analysis suggests that reservoir-based assessments may be inadequate for accurately estimating the risk of injection-induced seismicity, particularly where earthquakes are spatially decoupled from injection intervals.

Based on our results, we also suggest that it is unlikely that the small volume of CO_2 (40,000 tonnes) to be injected into the Arbuckle would induce the pore fluid pressure changes needed for failure, as similar small-scale injection has operated safely in the past in these counties and across Kansas. Rather, seismicity in Wellington Field and elsewhere in the region is more apt to occur where there are dense clusters of high-rate disposal wells. Under these commercial scale operations, high-rate injection into an aquifer not sealed from the basement, paired with conductive faults appears to be a recipe for induced seismicity (Barton et al., 1995; Morris et al., 2011; Zhang et al., 2013; Weingarten, 2015). However, the combination of good primary and secondary seals suggest that leakage into overlying fresh water aquifers is an unlikely scenario.

Lastly, the increasing need for safe disposal sites means that alternative reservoirs should be considered. We suggest that underpressured reservoirs like the Mississippian could be used for disposal and secondary/tertiary recovery methods, which could reduce the volume of fluid injected into the Arbuckle. In order to consider the Mississippian or other reservoirs for these purposes, the compatibility between produced brines and/or CO_2 with reservoir rocks, connate waters, and hydrocarbons would first need to be considered.

REFERENCES CITED

Aadnoy, B. S. (1990). In-situ stress directions from borehole fracture traces. Journal of Petroleum Science and Engineering, 4(2), 143-153.

Agbalaka, C. C., Dandekar, A. Y., Patil, S. L., Khataniar, S., and Hemsath, J. R. (2009). Coreflooding studies to evaluate the impact of salinity and wettability on oil recovery efficiency. Transport in Porous Media, 76(1), 77-94.

Alexeev, A., Shapiro, A., and Thomsen, K. (2015). Modeling of Dissolution Effects on Waterflooding. Transport in Porous Media, 106(3), 545-562.

Alt, R. C., and Zoback, M. D. (2015). A Detailed Oklahoma Stress Map for Induced Seismicity Mitigation. In AAPG Annual Convention and Exhibition.

Anderson, E. M. (1951). The dynamics of faulting and dyke formation with applications to Britain. Hafner Pub. Co.

Angelier, J. (1979). Determination of the mean principal directions of stresses for a given fault population. Tectonophysics, 56(3), T17-T26.

ANSS Catalog, United States Geological Survey, https://earthquake.usgs.gov/earthquakes/search/, (accessed 4/1/2016).

Baars, D. L., and Watney, W. L. (1991). Paleotectonic control of reservoir facies. Kansas Geological Survey. Bulletin, 233, 253-262.

Bachu, S. (2000). Sequestration of CO 2 in geological media: criteria and approach for site selection in response to climate change. Energy conversion and Management, 41(9), 953-970.

Bahorich, M., and Farmer, S. (1995). 3-D seismic discontinuity for faults and stratigraphic features: The coherence cube. The leading edge, 14(10), 1053-1058.

Baker, R. (1998). Reservoir management for waterfloods-Part II. Journal of Canadian Petroleum Technology, 37(01)

Barton, C. A., Zoback, M. D., and Moos, D. (1995). Fluid flow along potentially active faults in crystalline rock. Geology, 23(8), 683-686.

Bell, J. S., and Gough, D. I. (1979). Northeast-southwest compressive stress in Alberta evidence from oil wells. Earth and planetary science letters, 45(2), 475-482.

Bell, J. S. (1990). Investigating stress regimes in sedimentary basins using information from oil industry wireline logs and drilling records. Geological Society, London, Special Publications, 48(1), 305-325.

Benson, S. M., and Cole, D. R. (2008). CO2 sequestration in deep sedimentary formations. Elements, 4(5), 325-331.

Bhattacharya, S., Alan, P. B., and Paul, M. G. (2003). Cost-effective Integration of Geologic and Petrophysical Characterization with Material Balance and Decline Curve Analysis to Develop a 3D Reservoir Model for PC-based Reservoir Simulation to Design a Waterflood in a Mature Mississippian Carbonate Field with Limited Log Data. In AAPG Annual Meeting 2003.

Bradley, J. S. (1975). Abnormal formation pressure. AAPG Bulletin, 59(6), 957-973.

Brandt, H., and Tait, J. H. (1997). U.S. Patent No. 5,695,643. Washington, DC: U.S. Patent and Trademark Office.

Buchanan, R. C. (2015). Increased seismicity in Kansas. The Leading Edge, 34(6), 614-617.

Buckley, C. A., Simpson, A. E., Kerr, C. A., and Schutte, C. F. (1987). The treatment and disposal of waste brine solutions. Desalination, 67, 431-438.

Byerlee, J. (1978). Friction of rocks. Pure and applied geophysics, 116(4-5), 615-626.

Cappa, F., and Rutqvist, J. (2011). Impact of CO2 geological sequestration on the nucleation of earthquakes. Geophysical Research Letters, 38(17).

Carr, T. R., Merriam, D. F., and Bartley, J. D. (2005). Use of relational databases to evaluate regional petroleum accumulation, groundwater flow, and CO2 sequestration in Kansas. AAPG bulletin, 89(12), 1607-1627.

Chiaramonte, L., White, J. A., and Trainor-Guitton, W. (2015). Probabilistic geomechanical analysis of compartmentalization at the Snøhvit CO2 sequestration project. Journal of Geophysical Research: Solid Earth, 120(2), 1195-1209.

Cole, V. B. (1975). Subsurface Ordovician-Cambrian Rocks in Kansas. Reprinted 1981ed.) Lawrence, Kansas: Kansas Geological Survey, 2.

Dart, R. L. (1990). In situ stress analysis of wellbore breakouts from Oklahoma and the Texas Panhandle (No. 1866). Department of the Interior, US Geological Survey.

Ellsworth, W. L., and Zhonghuai, X. (1980). Determination of the stress tensor from focal mechanism data. Eos Trans AGU, 61(1), 117.

Ellsworth, W. L. (1982). A general theory for determining the state of stress in the earth from fault slip measurements. Terra Cognita, 2(2), 170.

Ellsworth, W. L. (2013). Injection-induced earthquakes. Science, 341(6142), 1225942.

Evans, D. M. (1966). The Denver area earthquakes and the Rocky Mountain Arsenal disposal well. Mountain Geologist, 3.

Evans, C. S., and Newell, K. D. (2013). The Mississippian Limestone Play in Kansas: Oil and Gas in a Complex Geologic Setting. Kansas Geological Survey, Geology Extension, University of Kansas.

Fazelalavi, M. (2016). Step-rate test, interference test results and DST results in Wellington, open file report. http://www.kgs.ku.edu/Publications/OFR/2015/OFR2015_20.pdf

Franseen, E. K. (2000). A review of Arbuckle Group strata in Kansas from a sedimentologic perspective: Insights for future research from past and recent studies. In Compass (Vol. 75, No. 2-3, pp. 68-89).

Franseen, E. K., Byrnes, A. P., Cansler, J. R., Steinhauff, D. M., Carr, T. R., and Dubois, M. K. (2003). Geological Controls on Variable Character of Arbuckle Reservoirs in Kansas: An Emerging Picture. The University of Kansas, Lawrence.

Franseen, E. K., Byrnes, A. P., Cansler, J. R., and Carr, T. (2004). The geology of Kansas: Arbuckle Group. Kansas Geological Survey.

Frohlich, C. (2012). Two-year survey comparing earthquake activity and injection-well locations in the Barnett Shale, Texas. Proceedings of the National Academy of Sciences, 109(35), 13934-13938.

Gephart, J. W., and Forsyth, D. W. (1984). An improved method for determining the regional stress tensor using earthquake focal mechanism data: application to the San Fernando earthquake sequence. Journal of Geophysical Research: Solid Earth, 89(B11), 9305-9320.

Gerhard, L. C. (2004). A new look at an old petroleum province. Kansas Geological Survey.

Goebel, E. D. (1966). Stratigraphy of Mississippian rocks in western Kansas: Kansas Univ., unpub (Doctoral dissertation, Ph. D. thesis).

Goebel, E. D. (1968). Mississippian rocks of western Kansas. AAPG Bulletin, 52(9), 1732-1778.

Grinestaff, G. H., and Caffrey, D. J. (2000). Waterflood management: A case study of the northwest fault block area of Prudhoe Bay, Alaska, using streamline simulation and traditional waterflood analysis. In SPE Annual Technical Conference and Exhibition. Society of Petroleum Engineers

Hanks, T. C., and Bakun, W. H. (2008). M-logA observations for recent large earthquakes. Bulletin of the Seismological Society of America, 98(1), 490-494.

Healy, J. H., Rubey, W. W., Griggs, D. T., and Raleigh, C. B. (1968). The Denver earthquakes. Science, 161(3848), 1301-1310.

Hildebrand, G. M., Steeples, D. W., Knapp, R. W., Miller, R. D., & Bennett, B. C. (1988). Microearthquakes in Kansas and Nebraska 1977–87. Seismological Research Letters, 59(4), 159-163.

Hillis, R. R., and Reynolds, S. D. (2000). The Australian stress map. Journal of the Geological Society, 157(5), 915-921.

Hinze, W. J. (1963). Regional gravity and magnetic anomaly maps of the Southern Peninsula of Michigan. Department of Conservation, Geological Survey Division.

Hinze, W. J., Wold, R. J., and O'Hara, N. W. (1982). 10: Gravity and magnetic anomaly studies of Lake Superior. Geological Society of America Memoirs, 156, 203-222.

Holland, A. A. (2013). Optimal fault orientations within Oklahoma. Seismological Research Letters, 84(5), 876-890.

Holubnyak, Y., Watney, W., Birdie, T., Rush, J., and Fazelalavi, M. (2016) Reservoir Modeling of CO2 Injection in Arbuckle Saline Aquifer at Wellington Field, Sumner County, Kansas, Kansas Geological Survey Open File Report, OFR 2016-29.

Horton, S. (2012). Disposal of hydrofracking waste fluid by injection into subsurface aquifers triggers earthquake swarm in central Arkansas with potential for damaging earthquake. Seismological Research Letters, 83(2), 250-260.

Keranen, K. M., Savage, H. M., Abers, G. A., and Cochran, E. S. (2013). Potentially induced earthquakes in Oklahoma, USA: Links between wastewater injection and the 2011 Mw 5.7 earthquake sequence. Geology, 41(6), 699-702.

Keranen, K. M., Weingarten, M., Abers, G. A., Bekins, B. A., and Ge, S. (2014). Sharp increase in central Oklahoma seismicity since 2008 induced by massive wastewater injection. Science, 345(6195), 448-451.

Keroher, R. P., and Kirby, J. J. (1948). Upper Cambrian and Lower Ordovician rocks in Kansas. University of Kansas publications.

KGS oil and gas wells database, Kansas Geological Survey, http://www.kgs.ku.edu/Magellan/Qualified/, (accessed 4/1/2016).

Kim, W. Y. (2013). Induced seismicity associated with fluid injection into a deep well in Youngstown, Ohio. Journal of Geophysical Research: Solid Earth, 118(7), 3506-3518.

King, E. R., and Zietz, I. (1971). Aeromagnetic study of the midcontinent gravity high of central United States. Geological Society of America Bulletin, 82(8), 2187-2208.

Koester, E. A. (1935). Geology of central Kansas uplift. AAPG Bulletin, 19(10), 1405-1426.

Kruger, J. M., 1997, On-line gravity and magnetic maps of Kansas: Kansas Geological Survey Open-File Report 96-51, http://www.kgs.ku.edu/PRS/PotenFld/potential.html. (Accessed 10/15/16).

Lee, W., and Girty, G. H. (1940). Subsurface Mississippian Rocks of Kansas. WC Austin, state printer.

Lee, W., Leatherock, C., and Botinelly, T. (1948), The stratigraphy and structural development of the Salina basin of Kansas: Kansas Geol. Survey Bull. 74, 155 p.

Lee, W., and Merriam, D. F. (1954). Preliminary Study of the Structure of Western Kansas. State Geological Survey of Kansas, University of Kansas.

Lee, W. (1956). Stratigraphy and structural development of the Salina basin area: Kansas Geol. Survey Bull. 121, 167 p.

Lugn, A. L. (1935) The Pleistocene Geology of Nebraska: Nebraska Geol. Survey, Bull. 10, pp. 1-223.

Lyons, P. L. (1959). The Greenleaf anomaly, a significant gravity feature. In Symposium on Geophysics in Kansas, WW Hambleton, ed.: Kansas Geological Survey, Bulletin137 (pp. 105-120).

McBee Jr, W. (2003). Nemaha strike-slip fault zone. In AAPG Mid-Continent Section Meeting (p. 14).

McKenzie, D. P. (1969). The relation between fault plane solutions for earthquakes and the directions of the principal stresses. Bulletin of the Seismological Society of America, 59(2), 591-601.

Merriam, D. F. (1956). History of earthquakes in Kansas. Bulletin of the Seismological Society of America, 46(2), 87-96.

Merriam, D. F. (1963). The geologic history of Kansas. University of Kansas publications.

McGarr, A. (1976). Seismic moments and volume changes. Journal of geophysical research, 81(8), 1487-1494.

McGarr, A. (2014). Maximum magnitude earthquakes induced by fluid injection. Journal of Geophysical Research: solid earth, 119(2), 1008-1019.

McKenzie, D. P. (1969). The relation between fault plane solutions for earthquakes and the directions of the principal stresses. Bulletin of the Seismological Society of America, 59(2), 591-601.

Melrose, J. C., and Brandner, C.F. (1974). Role of capillary forces in determining microscopic displacement efficiency for oil recovery by waterflooding. Journal of Canadian Petroleum Technology, 13(04).

Midwest Governors Association and Great Plains Institute. (2012). CO2-EOR potential in the MGA region. http://docplayer.net/15151292-Co2-eor-potential-in-the-mga-region.html (Accessed 10/21/2016)

Michael, A. J. (1984). Determination of stress from slip data: faults and folds. Journal of Geophysical Research: Solid Earth, 89(B13), 11517-11526.

Michael, A. J. (1987). Use of focal mechanisms to determine stress: a control study. Journal of Geophysical Research: Solid Earth, 92(B1), 357-368.

Moos, D., and Zoback, M. D. (1990). Application to Continental, Deep Sea Drilling Project, and. Journal of Geophysical Research, 95(B6), 9305-9325.

Morris, A., Ferrill, D. A., and Henderson, D. B. (1996). Slip-tendency analysis and fault reactivation. Geology, 24(3), 275-278.

Morris, W., Leung, B., Furukawa, H., Yaghi, O. K., He, N., Hayashi, H., ... and Yaghi, O. M. (2010). A combined experimental− computational investigation of carbon dioxide capture in a series of isoreticular zeolitic imidazolate frameworks. Journal of the American Chemical Society, 132(32), 11006-11008.

Morris, J. P., Hao, Y., Foxall, W., and McNab, W. (2011). A study of injection-induced mechanical deformation at the In Salah CO 2 storage project. International Journal of Greenhouse Gas Control, 5(2), 270-280.

Morrow, N. R. (1990). Wettability and its effect on oil recovery. Journal of Petroleum Technology, 42(12), 1-476.

Nasralla, R. A., Snippe, J. R., and Farajzadeh, R. (2015, August). Coupled Geochemical-Reservoir Model to Understand the Interaction Between Low Salinity Brines and Carbonate Rock. In SPE Asia Pacific Enhanced Oil Recovery Conference. Society of Petroleum Engineers.

Nelson, E. J., Chipperfield, S. T., Hillis, R. R., Gilbert, J., McGowen, J., and Mildren, S. D. (2007). The relationship between closure pressures from fluid injection tests and the minimum principal stress in strong rocks. International Journal of Rock Mechanics and Mining Sciences, 44(5), 787-801.

Nelson, P. H., and Gianoutsos, N. J. (2011). Evolution of overpressured and underpressured oil and gas reservoirs, Anadarko Basin of Oklahoma, Texas, and Kansas (No. 2011-1245). US Geological Survey.

Newell, K. D., Watney, W. L., Cheng, W. L., and Brownrigg, R. L. (1987). Stratigraphic and spatial distribution of oil and gas production in Kansas.

Oray, E., Hinze, W. J., and O'Hara, N.O., (1973). Gravity and magnetic evidence for the eastern termination of the Lake Superior syncline. Geological Society of America Bulletin, 84(8), 2763-2780.

Puckette, J., and Al-Shaieb, Z. (2003). Naturally underpressured reservoirs: applying the compartment concept to the safe disposal of liquid waste.

Raleigh, C. B., Healy, J. H., and Bredehoeft, J. D. (1976). An experiment in earthquake control at Rangely, Colorado. work (Fig. Ib), 108(52), 30.

Reasenberg, P. A., and Simpson, R. W. (1992). Response of regional seismicity to the static stress change produced by the Loma Prieta earthquake. Science, 255(5052), 1687.

Rubinstein, J. L., Ellsworth, W. L., McGarr, A., and Benz, H. M. (2014). The 2001–present induced earthquake sequence in the Raton Basin of northern New Mexico and southern Colorado. Bulletin of the Seismological Society of America.

Scheffer, A. (2012). Geochemical and Microbiological Characterization of the Arbuckle Saline Aquifer, a Potential CO2 Storage Reservoir; Implications for Hydraulic Separation and Caprock Integrity (Doctoral dissertation, University of Kansas).

Seeber, L., and Armbruster, J. G. (2000). Earthquakes as beacons of stress change. Nature, 407(6800), 69-72.

Shipton, Z. K., Evans, J. P., Dockrill, B., Heath, J., Williams, A., Kirchner, D., and Kolesar, P. T. (2006). Natural leaking CO2-charged systems as analogs for failed geologic storage reservoirs. Carbon Dioxide Capture for Storage in Deep Geologic Formations–Results from the CO2 Capture Project, 699-712.

Smithson, S. B. (1971). Densities of metamorphic rocks. Geophysics, 36(4), 690-694.

Sorenson, R. P. (2005). A dynamic model for the Permian Panhandle and Hugoton fields, western Anadarko basin. AAPG bulletin, 89(7), 921-938.

Stander, T. W., and Grant, J. L. (1989). A case history of petroleum exploration in the southern Forest City basin using gravity and magnetic surveys. Bulletin-State Geological Survey of Kansas, (226-228), 245.

Steeples, D. W., DuBois, S. M., and Wilson, F. W. (1979). Seismicity, faulting, and geophysical anomalies in Nemaha County, Kansas: Relationship to regional structures. Geology, 7(3), 134-138.

Steeples, D. W., and Brosius, L. (1996). Earthquakes: Kansas Geological Survey. Public Information Circular, 3(5).

Stein, R. S. (1999). The role of stress transfer in earthquake occurrence. Nature, 402(6762), 605-609.

Stein, S., and Wysession, M. (2009). An introduction to seismology, earthquakes, and earth structure. John Wiley and Sons.

Streit, J. E., and Hillis, R. R. (2004). Estimating fault stability and sustainable fluid pressures for underground storage of CO 2 in porous rock. Energy, 29(9), 1445-1456.

Tang, G. Q., and Morrow, N. R. (1997). Salinity, temperature, oil composition, and oil recovery by waterflooding. SPE Reservoir Engineering, 12(04), 269-276.

Thiel, E. (1956). Correlation of gravity anomalies with the Keweenawan geology of Wisconsin and Minnesota. Geological Society of America Bulletin, 67(8), 1079-1100.

Tingay, M., Reinecker, J., and Müller, B. (2008). Borehole breakout and drilling-induced fracture analysis from image logs. World Stress Map Project, 1-8.

Townend, J., and Zoback, M. D. (2000). How faulting keeps the crust strong. Geology, 28(5), 399-402.

Vavryčuk, V. (2014). Iterative joint inversion for stress and fault orientations from focal mechanisms. Geophysical Journal International, 199(1), 69-77.

Vilarrasa, V., Olivella, S., Carrera, J., and Rutqvist, J. (2014). Long term impacts of cold CO 2 injection on the caprock integrity. International Journal of Greenhouse Gas Control, 24, 1-13.

Walters, R. F. (1958). Differential entrapment of oil and gas in Arbuckle dolomite of central Kansas. AAPG Bulletin, 42(9), 2133-2173.

Watney, W. L., Guy, W. J., and Byrnes, A. P. (2002). Characterization of the Mississippian Osage chat in south-central Kansas: Kansas Geological Survey, Open-file Report 2002-50.

Watney, L. (2016). Personal communication.

Weingarten, M., Ge, S., Godt, J. W., Bekins, B. A., and Rubinstein, J. L. (2015). High-rate injection is associated with the increase in US mid-continent seismicity. Science, 348(6241), 1336-1340.

Wells, D. L., and Coppersmith, K. J. (1994). New empirical relationships among magnitude, rupture length, rupture width, rupture area, and surface displacement. Bulletin of the seismological Society of America, 84(4), 974-1002.

Wiprut, D., and Zoback, M. (2000). Constraining the stress tensor in the Visund field, Norwegian North Sea: Application to wellbore stability and sand production. International Journal of Rock Mechanics and Mining Sciences, 37(1), 317-336.

Woelk, T. S., and Hinze, W. J. (1995). Midcontinent Rift System in Northeastern Kansas. Bulletin – Kansas geological survey, 22-27.

Worum, G., van Wees, J. D., Bada, G., van Balen, R. T., Cloetingh, S., and Pagnier, H. (2004). Slip tendency analysis as a tool to constrain fault reactivation: A numerical approach applied to three-dimensional fault models in the Roer Valley rift system (southeast Netherlands). Journal of Geophysical Research: Solid Earth, 109(B2).

Yih-Hsiung, Y., Eric, B., Lin, C. H., and Jacques, A. (1991). Stress tensor analysis in the Taiwan area from focal mechanisms of earthquakes. Tectonophysics, 200(1), 267-280.

Zeller, D. E. (1968). Stratigraphic succession in Kansas. Kansas Geological Survey Bulletin, 189. http://www.kgs.ku.edu/Publications/Bulletins/189/ (accessed 10/15/2016)

Zhang, Y., Person, M., Rupp, J., Ellett, K., Celia, M. A., Gable, C. W., ... and Dewers, T. (2013). Hydrogeologic controls on induced seismicity in crystalline basement rocks due to fluid injection into basal reservoirs. Groundwater, 51(4), 525-538.

Zoback, M. L., and Zoback, M. (1980). State of stress in the conterminous United States. Journal of Geophysical Research: Solid Earth, 85(B11), 6113-6156.

Zoback, M. D., Moos, D., Mastin, L., and Anderson, R. N. (1985). Well bore breakouts and in situ stress. Journal of Geophysical Research: Solid Earth, 90(B7), 5523-5530.

Zoback, M., Zoback, M., Eaton, J., Mount, V., and Suppe, J. (1987). New evidence on the state of stress of the San Andreas fault system. Science, 238(4830), 1105-1111.

Zoback, M. L., Zoback, M. D., Adams, J., Assumpcao, M., Bell, S., Bergman, E. A., and Fuchs, K. (1989). Global patterns of tectonic stress. Nature, 341(6240), 291-298.

Zoback, M. D., Zoback, M. L., Slemmons, D. L., Engdahl, E. R., Zoback, M. D., and Blackwell, M. L. (1991). Neotectonics of North America. Geol. Soc. Am., Boulder, CO, 339-366.

Zoback, M. L. (1992). First-and second-order patterns of stress in the lithosphere: The World Stress Map Project. Journal of Geophysical Research: Solid Earth, 97(B8), 11703-11728.

Zoback, M. D., Townend, J., and Grollimund, B. (2002). Steady-state failure equilibrium and deformation of intraplate lithosphere. International Geology Review, 44(5), 383-401.

Zoback, M. D., Barton, C. A., Brudy, M., Castillo, D. A., Finkbeiner, T., Grollimund, B. R., ... and Wiprut, D. J. (2003). Determination of stress orientation and magnitude in deep wells. International Journal of Rock Mechanics and Mining Sciences, 40(7), 1049-1076.

Zoback, M. D., and Gorelick, S. M. (2012). Earthquake triggering and large-scale geologic storage of carbon dioxide. Proceedings of the National Academy of Sciences, 109(26), 10164-10168.

FIGURE CAPTIONS

Figure 1. Earthquake data M>1 (grey circles; N=3903), including earthquake moment tensor solutions (N=70) for M3.0 (small circle) and M4.0 (large circle) earthquakes, were collected from USGS-ANSS from 1/12-4/16 for south central Kansas and north central Oklahoma (inset A). Earthquakes are in close proximity to high rate injection wells (red triangles). The study area, located in Wellington field, Sumner County, Kansas has 2-CO_2 injection wells for simulating EOR (1-32) and long-term storage (1-28). Inset B shows 3D seismic data boundaries around Wellington field to the south and Anson Bates field to the north, with 12-projected fault planes and the location of the two proposed injection wells. Stress orientations and magnitudes were estimated using image log (blue stars) and density log data (orange stars) from wells in Barber, Harper, Sumner, and Cowley counties including wells KGS 1-28 and KGS 1-32, which had both density and image logs.

Figure 2. The average injection rate per disposal well increased significantly in 2012 in response to increased demand for wastewater disposal operations in the Midcontinent. Consequently, seismicity near the injections wells in Harper and Sumner county has increased significantly since 2013 (red bars; M 2.0+) (Buchanan, 2015).

Figure 3. Stratigraphic column showing major stratigraphic units across Kansas. Modified from Carr et al. (2005).

Figure 4. Schematic diagram showing the development of bore hole breakouts and drilling induced fractures relative to the maximum (σH) and minimum (σh) horizontal stresses. Drilling induced tensile fractures occur parallel to the orientation of SHmax and borehole breakouts occur perpendicular to the orientation of SHmax. Figure modified from Tingay et al. (2008) and Hillis and Reynolds (2000).

Figure 5. (Left) Map view of study area with projected fault planes (solid lines). The depth slice was taken at the top of the Arbuckle at -871 m (TVDSS) and shows amplitude highs (red) and lows (blue), including areas of abrupt amplitude change, representing potential faults. Fault 7 is in close proximity to the proposed injection wells, and is at the highest risk for reactivation.

(Right) Vertical seismic profile (A-A'; 3x vertical exaggeration) showing amplitude highs (red) and lows (blue), with mapped faults 1, 2, and 3, and slip direction, as well as mapped stratigraphic horizons. Faults were mapped by identifying offsetting stratigraphic horizons and breaks in amplitude. The top of the Mississippian, KC Limestone, and Topeka Limestone were not cut by the underlying faults. Faults 1, 2, and 3 clearly cut the top basement reflector and appear to continue beyond the boundaries of the data.

Figure 6. 3D model of the study area looking to the NE. The model shows the location and geometry of 12 subsurface faults, 5 major mapped stratigraphic horizons, and the 2 proposed well locations (3x vertical exaggeration). Faults are oriented ~NNE (Table 1). The majority of faults, excluding fault 9, terminate at the top of the Mississippian and cut the Arbuckle. Although seismic data quality diminishes below the Arbuckle, faults 1, 2, and 3 clearly cut the top basement reflector and could be potential pathways for fluid flow to greater depths.

Figure 7. Natural open fracture orientations at KGS 1-28 and KGS 1-32. Fracture orientations vary, with the majority ranging from 010° to 040°. This range in azimuth is consistent with optimally oriented faults in the study area, and suggest that the modeled faults could also be conductive.

Figure 8. (Top) Image log from well 1-32 generated through microresistivity measurements of low conductivity (bright) and high conductivity (dark) areas. Drilling-induced tensile fractures are identified from image logs as highly conductive features running vertical along the wellbore wall with 180° separation. Drilling induced fractures are consistent with the maximum horizontal stress (SHmax) direction. (Bottom) Rose diagram of 40 drilling induced tensile fractures, based on 80 total measurements taken from 4 wells in south-central Kansas. SHmax measurements ranged from 055° to 087° with an average of 077° and a standard deviation of 007°.

Figure 9. Results of stress inversion of earthquake moment tensor solutions. Data was collected from USGS-ANSS from south-central Kansas and north-central Oklahoma from 01/12-04/16. Both strike-slip (n=39) and normal-slip (n=31) moment tensor solutions were collected and were inverted separately. Average estimate for SHmax ranged from 080° (SS) - 070° (NS) with an overall average of ~075°. Plots were created using STRESSInverse software based on the method proposed by Michael (1984, 1987) (Vavryčuk, V., 2014).

Figure 10. Stress gradients based on 11-density logs (Sv), 2-step rate tests (Shmin), and estimates based on the presence of drilling induced tensile fractures (SHmax). Fracture closure pressure was determined from step rate test data from KGS 1-32 and is the consistent with the magnitude of Shmin. Measurements were taken at gauge depth of 1,484 m. Pore pressure was estimated using a fresh water hydrostatic gradient (9.8 MPa/km).

Figure 11. Stress polygon showing possible stress magnitudes for SHmax and Shmin for different stress environments (strike-slip, normal, and reverse) for an estimated Sv magnitude of 155 MPa. Estimations were made for a depth of 5.85 km, the average depth of NEIC reported induced events in south-central Kansas. Polygon boundaries represent a state of failure for optimally oriented faults. For a strike-slip stress state, an intermediate value for SHmax and

Shmin was used for the slip tendency analysis. For a normal slip stress state, an intermediate value for SHmax was used for the slip tendency analysis.

Figure 12. Slip tendency analysis for faults at Mississippian depth (1,120 m) in a strike-slip stress state. Slip tendency values are projected on the modeled faults (A & B) and show that the majority of faults are stable with only some faults with areas that are optimally oriented for failure. Fault planes were then projected into Mohr circle space with failure envelopes for coefficient of friction of 0.5 and 0.6 (C). Increasing the pore fluid pressure by 1.1 to 4.13 MPa brings a number of optimally oriented faults into failure (D).

Figure 13. Slip tendency analysis for faults at Mississippian depth (1,120 m) in a normal slip stress state. Slip tendency values are projected on the modeled faults (A & B) and show that the majority of faults are stable. Fault planes were then projected into Mohr circle space with failure envelopes for coefficient of friction of 0.5 and 0.6 (C). Increasing the pore fluid pressure by 5.79 to 7.60 MPa brings any optimally oriented faults into failure (D).

Figure 14. Slip tendency analysis for faults at Arbuckle depth (1,484 m) in a strike-slip stress state. Slip tendency values are projected on the modeled faults (A & B) and show that the majority of faults are stable with only some faults with areas that are optimally oriented for failure. Fault planes were then projected into Mohr circle space with failure envelopes for coefficient of friction of 0.5 and 0.6 (C). Increasing the pore fluid pressure by 1.31 to 5.37 MPa brings a number of optimally oriented faults into failure (D).

Figure 15. Slip tendency analysis for faults at Arbuckle depth (1,484 m) in a normal slip stress state. Slip tendency values are projected on the modeled faults (A & B) and show that the majority of faults are stable. Fault planes were then projected into Mohr circle space with failure envelopes for coefficient of friction of 0.5 and 0.6 (C). Increasing the pore fluid pressure by 7.0 to 9.8 MPa brings any optimally oriented faults into failure (D).

Figure 16. Slip tendency analysis for faults at basement depth (5,850 m) in a strike-slip stress state. Slip tendency values are projected on the modeled faults (A & B) and show that, assuming a critically stressed crust, portions of 3 faults are already at failure and would slip in response to even small changes in pore pressure (C). Slip tendency values were calculated using an estimated stress state as determined by the stress polygon (Figure 10).

Figure 17. Slip tendency analysis for faults at basement depth (5,850 m) in a normal slip stress state. Slip tendency values are projected on the modeled faults (A & B) and show that the majority of faults are stable. Fault planes were then projected into Mohr circle space with a failure envelope for coefficient of friction of 0.6 (C). Any optimally oriented faults would already be at failure, however, none of the modeled faults are optimally oriented. An additional increase in pore fluid pressure of 5.44 MPa would be required to bring faults into failure (D).

Figure 18. Slip tendency uncertainty was calculated for measurements taken at Arbuckle depth (1,484 m) for both SS and NS stress states. Shmin was reduced by 10%, 20%, and 30%, and the resulting slip tendency was recorded. Results showed that slip tendency increases with reduced magnitudes of Shmin.

Table 1. Fault Characterization

Fault #	Strike (°)	Dip (°)	Length (m)	Width (m)	Vertical Separation (m)
1	6	90	4450+	883+	22
2	13	90	2173	914+	30
3	12	90	4267+	990+	33
4	165	70SE	290	99	21
5	11	71.5E	1441	98	29
6	10	88W	210	206	25
7	26	75SE	2652	411	22
8	166	86SW	930	274	12
9	170	75E	303	274	22
10	17	83SE	503	274	18
11	145	80SW	396	414	12
12	13	51SE	945	62	22

Table 2. Drilling Induced Tensile Fractures

McGrath 1-16 (C)			**Spriggs 1-34 (B)**			**Sumner 1-28 (C)**			**Sumner 1-32 (C)**		
Azimuth #1 (°)	Azimuth #2 (°)	Height (m)	Azimuth #1 (°)	Azimuth #2 (°)	Height (m)	Azimuth #1 (°)	Azimuth #2 (°)	Height (m)	Azimuth #1 (°)	Azimuth #2 (°)	Height (m)
81	86	3	79	84	2	79	80	30	66	71	40
81	81	5	79	61	3	81	81	2	78	66	35
76	81	4	81	84	2	63	80	12	55	76	15
81	81	2	79	59	1	73	79	11	71	77	43
83	81	6	78	76	3	77	79	3	66	81	200
81	81	4	71	74	3						
81	81	1	79	80	5						
81	81	2	77	79	2						
84	81	2	83	81	7						
83	79	4	71	72	29						
82	82	1	79	81	21						
81	87	4	76	81	5						
81	80	5	61	71	7						
84	84	26	83	87	14						
81	81	6	63	71	21						

Table 3. Moment tensor nodal planes for inversion

Strike-Slip				**Normal-Slip**			
Location	Strike(°)	Dip(°)	Rake(°)	Location	Strike(°)	Dip(°)	Rake(°)
36.827°N 97.775°W	48	85	160	36.939°N 97.797°W	85	60	-65
36.918°N 97.982°W	36	80	-175	36.831°N 98.274°W	80	65	-60
36.751°N 98.056°W	219	75	-173	36.944°N 97.831°W	265	70	-75
36.818°N 98.285°W	224	60	-145	36.946°N 97.811°W	260	75	-60
37.122°N 97.617°W	206	74	167	36.838°N 98.276°W	72	26	-75
37.152°N 97.623°W	0	90	160	36.941°N 97.826°W	82	62	-76
36.735°N 97.840°W	50	90	-175	36.948°N 97.828°W	85	54	-73
36.842°N 97.827°W	217	73	-162	36.947°N 97.826°W	100	65	-55
36.831°N 97.801°W	35	64	-162	36.946°N 97.835°W	80	65	-60
36.746°N 98.224°W	244	80	-179	36.947°N 97.837°W	105	58	-47
36.849°N 97.698°W	238	86	-171	36.953°N 97.855°W	94	60	-51
36.818°N 97.285°W	224	60	-145	37.057°N 97.934°W	59	62	-112
36.849°N 97.880°W	61	85	-165	37.054°N 97.941°W	61	52	-102
36.945°N 97.631°W	51	64	180	36.844°N 98.269°W	43	45	-123
37.105°N 97.650°W	6	86	-179	36.837°N 98.245°W	53	40	-116
36.751°N 97.534°W	200	85	-175	36.846°N 98.252°W	38	46	-129
37.187°N 97.900°W	180	80	-5	36.842°N 98.259°W	65	26	-107
36.815°N 98.291°W	20	67	-167	37.265°N 97.921°W	76	25	-83
37.189°N 97.901°W	44	60	-145	37.041°N 97.905°W	63	51	-124
36.945°N 97.630°W	60	85	20	36.952°N 97.624°W	288	50	-94
36.808°N 98.364°W	230	81	172	36.871°N 98.127°W	82	24	-86
37.185°N 97.856°W	30	80	180	36.873°N 98.335°W	84	37	-62
36.952°N 97.615°W	24	75	168	37.229°N 98.033°W	103	37	-54
36.807°N 98.360°W	44	76	154	37.245°N 97.955°W	81	48	-81
36.803°N 98.196°W	198	75	-153	37.221°N 97.963°W	87	34	-67
37.215°N 97.872°W	212	51	-164	36.821°N 97.722°W	34	37	-108
36.762°N 98.054°W	35	78	154	36.840°N 98.254°W	86	33	-76
36.820°N 97.719°W	24	72	-173	36.841°N 98.278°W	93	33	-63
37.271°N 97.621°W	22	66	-175	37.132°N 97.768°W	57	48	-59
37.263°N 97.635°W	355	65	-30	36.958°N 97.670°W	105	62	-113
36.858°N 97.871°W	30	84	-156	37.130°N 97.776°W	251	64	-62
36.852°N 97.869°W	203	80	-166				
36.861°N 97.873°W	24	86	166				
36.762°N 98.044°W	218	75	-170				
36.750°N 98.045°W	46	64	-146				
36.756°N 98.045°W	227	71	-149				
36.868°N 97.688°W	45	90	180				
36.851°N 97.856°W	205	90	175				
37.192°N 97.899°W	193	72	-154				

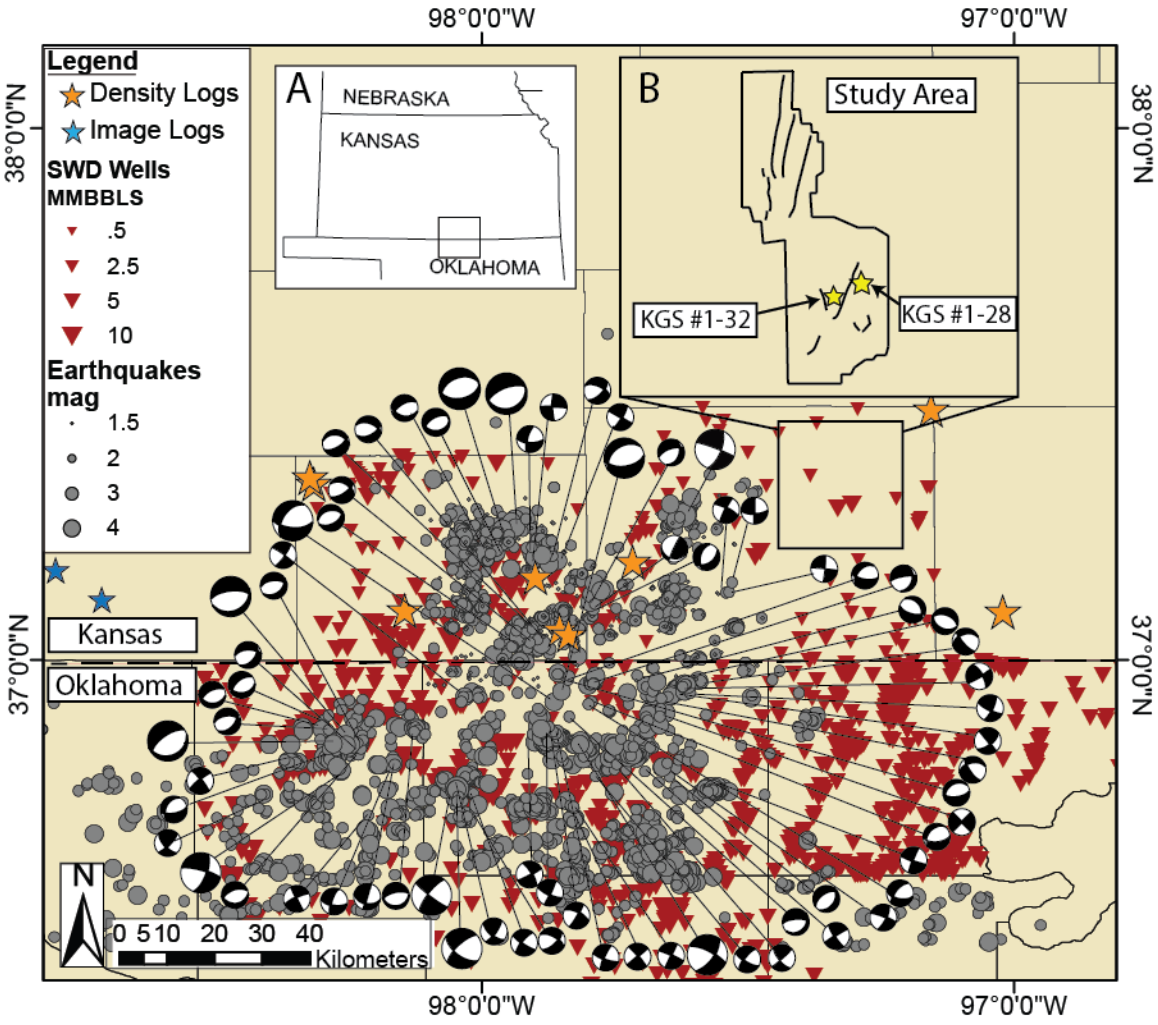
98°0'0"W
97°0'0"W
38°0'0"N
37°0'0"N
Legend
Density Logs
Image Logs
SWD Wells
MMBBLS
.5
2.5
5
10
Earthquakes
mag
1.5
2
3
4
A
NEBRASKA
KANSAS
OKLAHOMA
B
Study Area
KGS #1-32
KGS #1-28
Kansas
Oklahoma
N
0 5 10 20 30 40
Kilometers

Figure 1

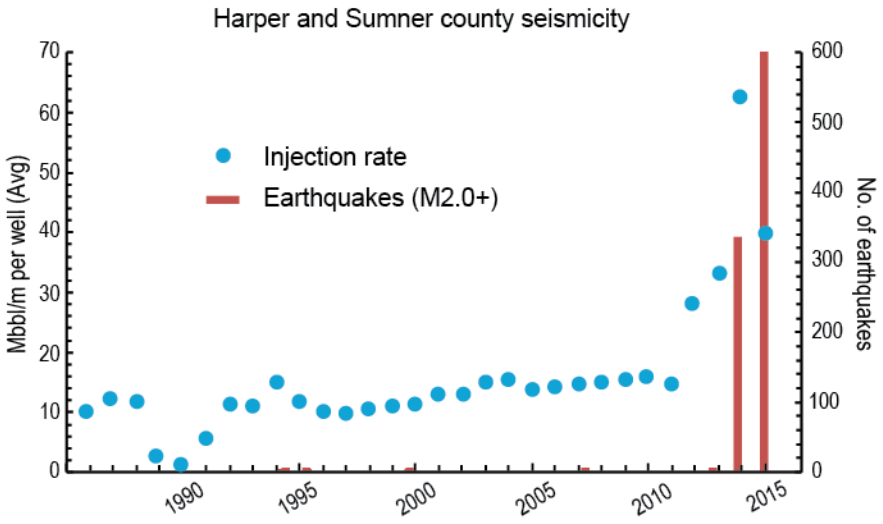
Harper and Sumner county seismicity
Injection rate
Earthquakes (M2.0+)
Mbbl/m per well (Avg)
No. of earthquakes
0
10
20
30
40
50
60
70
0
100
200
300
400
500
600
1990
1995
2000
2005
2010
2015

Figure 2

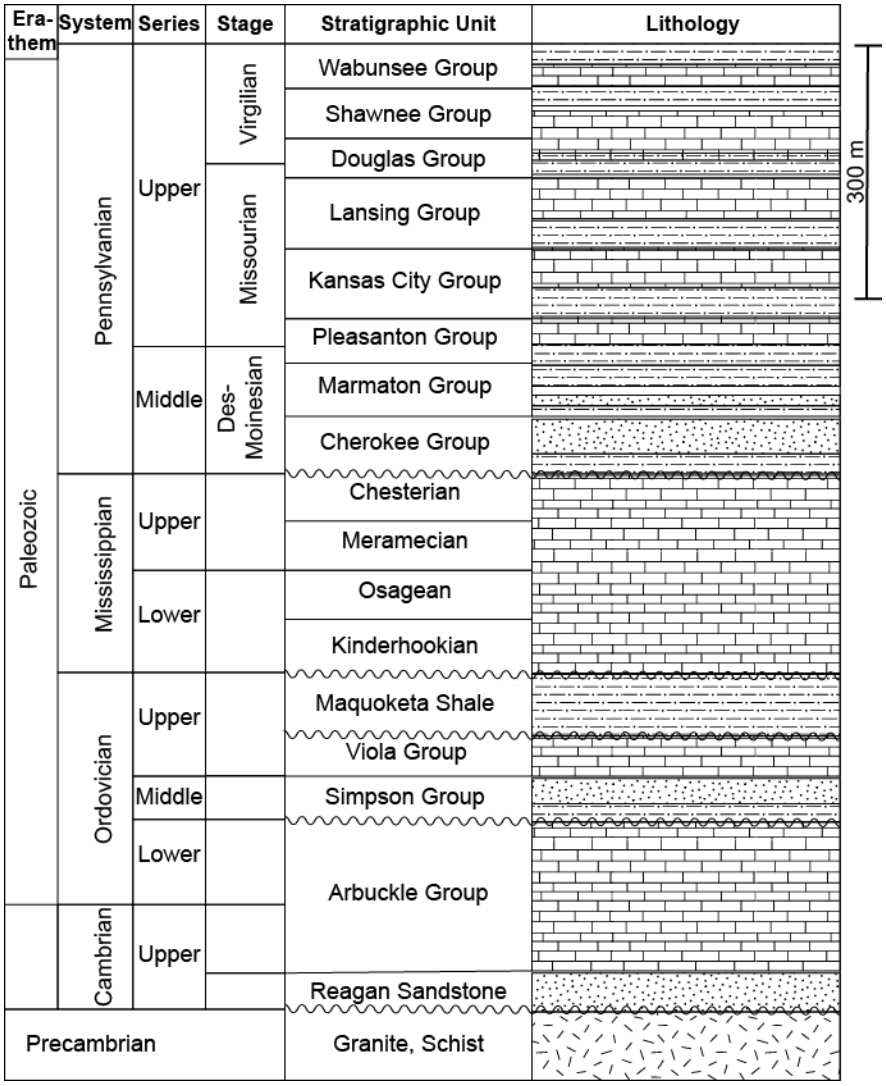
Era-them
System
Series
Stage
Stratigraphic Unit
Lithology
Paleozoic
Pennsylvanian
Upper
Virgilian
Missourian
Middle
Des-Moinesian
Mississippian
Upper
Lower
Ordovician
Upper
Middle
Lower
Cambrian
Upper
Precambrian
Wabunsee Group
Shawnee Group
Douglas Group
Lansing Group
Kansas City Group
Pleasanton Group
Marmaton Group
Cherokee Group
Chesterian
Meramecian
Osagean
Kinderhookian
Maquoketa Shale
Viola Group
Simpson Group
Arbuckle Group
Reagan Sandstone
Granite, Schist
300 m

Figure 3

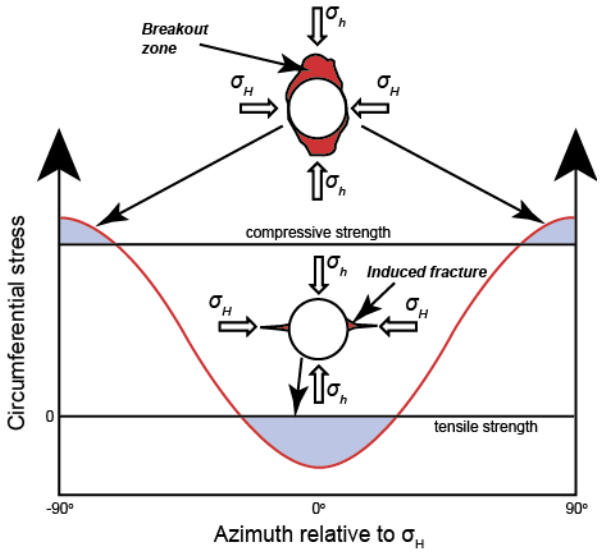
Breakout zone
σh
σH
σH
σh
compressive strength
σh
Induced fracture
σH
σH
σh
0
tensile strength
Circumferential stress
-90°
0°
90°
Azimuth relative to σH

Figure 4

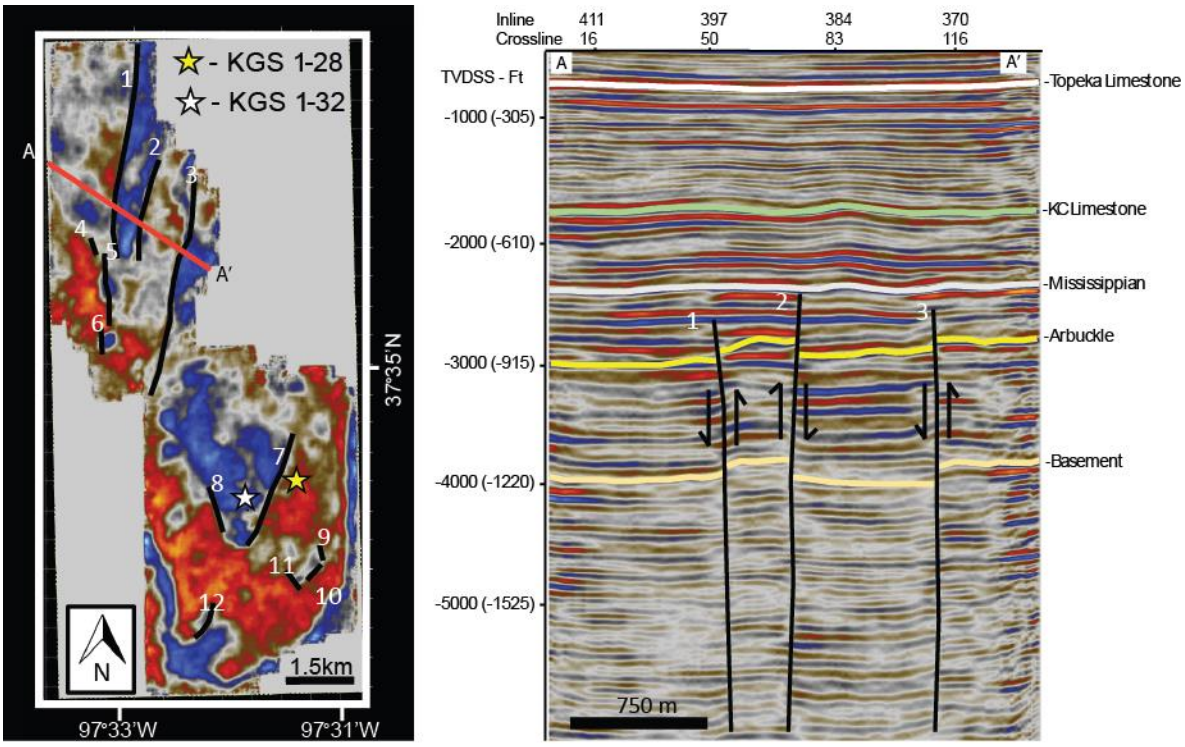
- KGS 1-28
- KGS 1-32
A
A′
1
2
3
4
5
6
7
8
9
10
11
12
N
1.5km
37°35'N
97°33'W
97°31'W
Inline 411 397 384 370
Crossline 16 50 83 116
TVDSS - Ft
-1000 (-305)
-2000 (-610)
-3000 (-915)
-4000 (-1220)
-5000 (-1525)
-Topeka Limestone
-KC Limestone
-Mississippian
-Arbuckle
-Basement
750 m

Figure 5

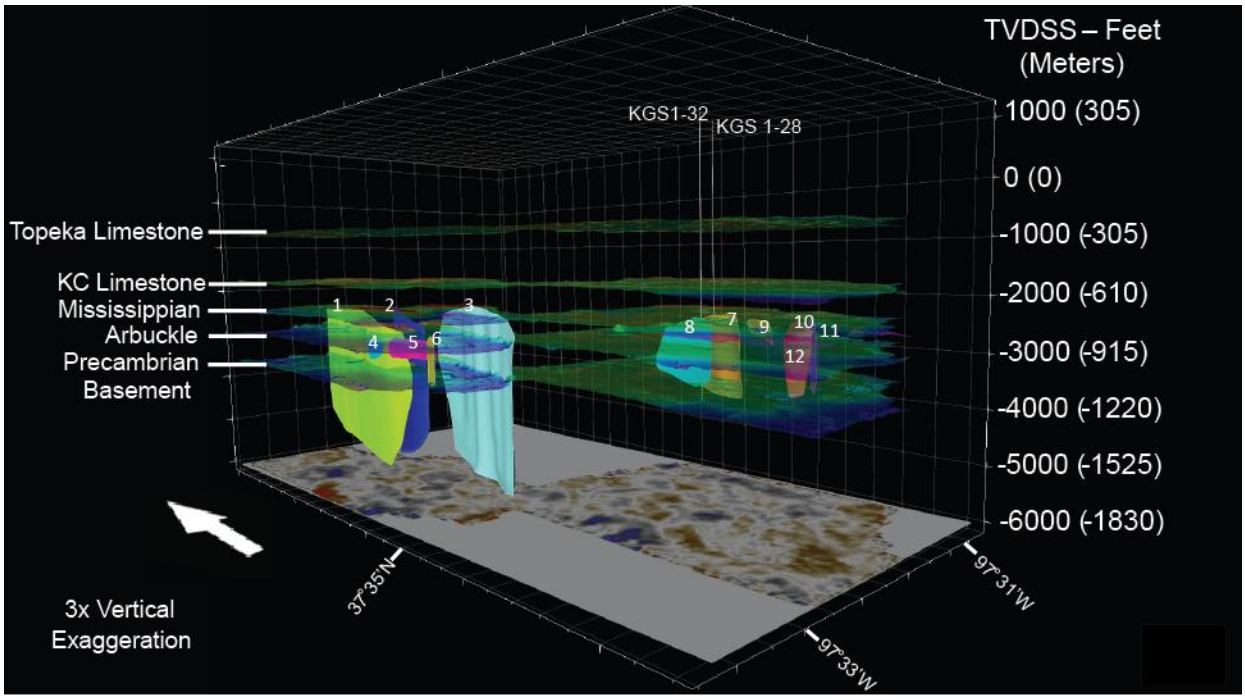
TVDSS – Feet
(Meters)
1000 (305)
0 (0)
-1000 (-305)
-2000 (-610)
-3000 (-915)
-4000 (-1220)
-5000 (-1525)
-6000 (-1830)
KGS1-32
KGS 1-28
Topeka Limestone
KC Limestone
Mississippian
Arbuckle
Precambrian
Basement
1
2
3
4
5
6
7
8
9
10
11
12
37°35'N
97°31'W
97°33'W
3x Vertical
Exaggeration

Figure 6

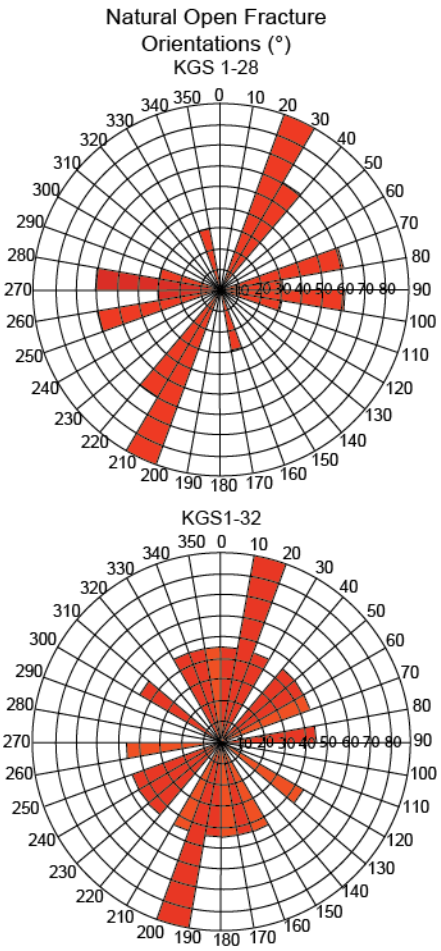

Figure 7

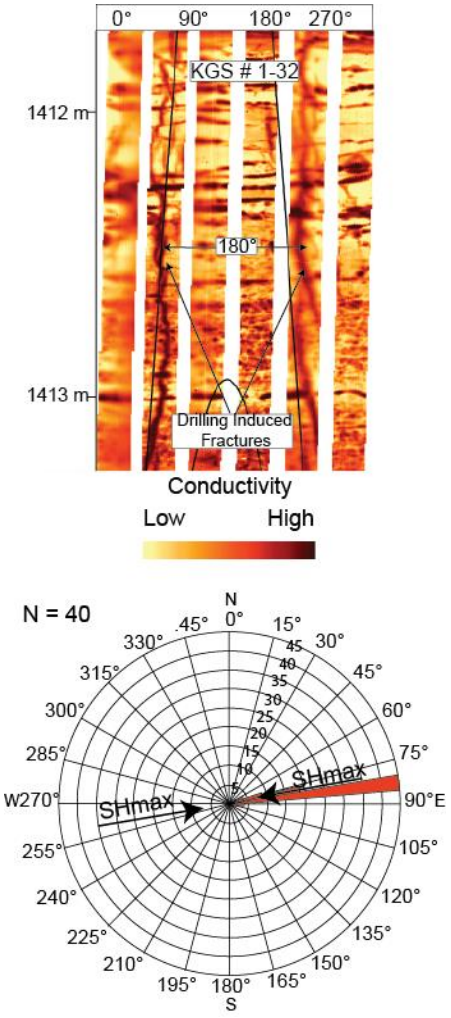
0°
90°
180°
270°
KGS # 1-32
1412 m
180°
1413 m
Drilling Induced Fractures
Conductivity
Low
High
N = 40
N
0°
15°
30°
45°
60°
75°
90°E
105°
120°
135°
150°
165°
180°
S
195°
210°
225°
240°
255°
W270°
285°
300°
315°
330°
345°
45
40
35
30
25
20
15
10
5
SHmax
SHmax

Figure 8

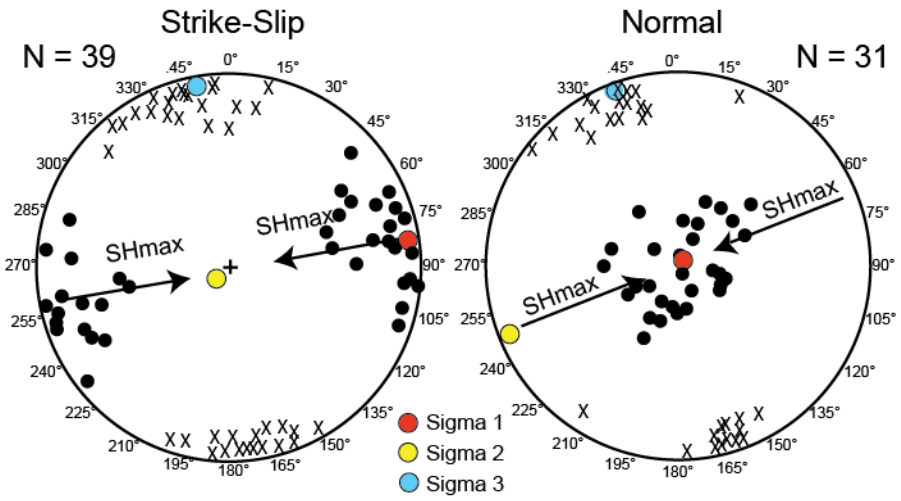
Strike-Slip
N = 39
Normal
N = 31
SHmax
SHmax
SHmax
SHmax
Sigma 1
Sigma 2
Sigma 3

Figure 9

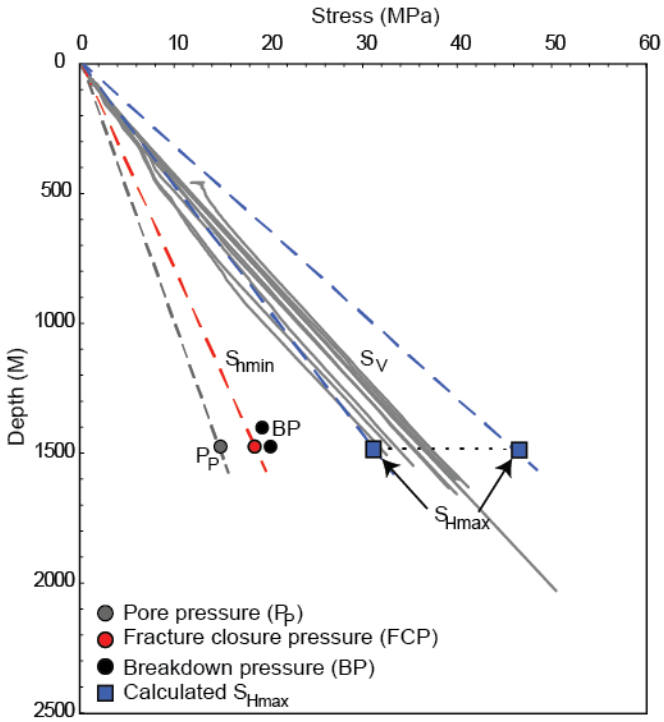
Stress (MPa)
0
10
20
30
40
50
60
0
500
1000
1500
2000
2500
Depth (M)
S_{hmin}
S_V
BP
P_P
S_{Hmax}
Pore pressure (P_P)
Fracture closure pressure (FCP)
Breakdown pressure (BP)
Calculated S_{Hmax}

Figure 10

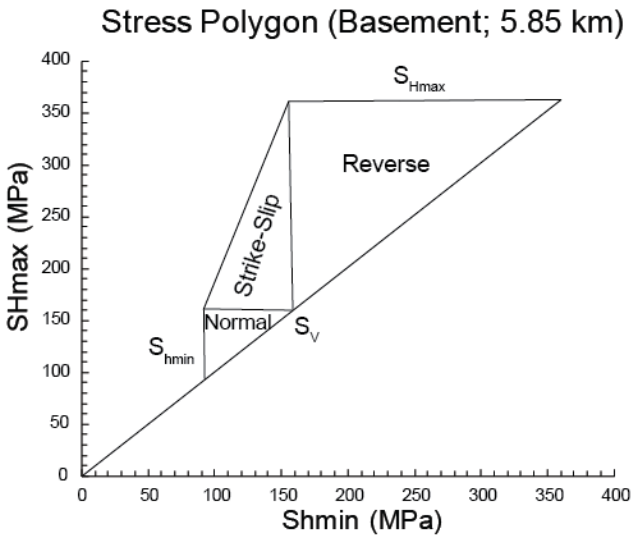
Stress Polygon (Basement; 5.85 km)
SHmax (MPa)
Shmin (MPa)
0
50
100
150
200
250
300
350
400
S Hmax
Reverse
Strike-Slip
Normal
S V
S hmin

Figure 11

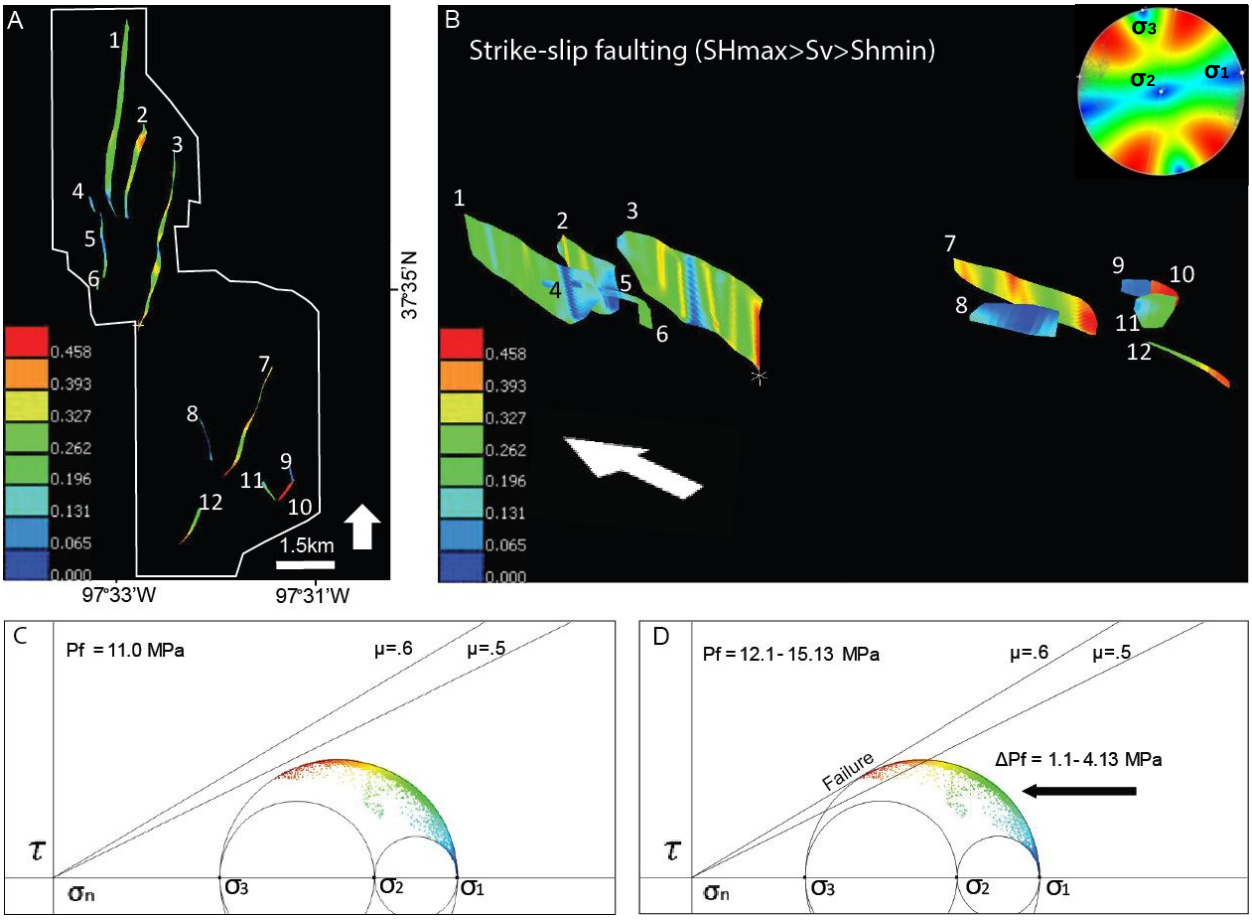
A
1
2
3
4
5
6
7
8
9
10
11
12
0.458
0.393
0.327
0.262
0.196
0.131
0.065
0.000
1.5km
97°33'W
97°31'W
37°35'N
B
Strike-slip faulting (SHmax>Sv>Shmin)
σ3
σ2
σ1
C
Pf = 11.0 MPa
μ=.6
μ=.5
τ
σn
σ3
σ2
σ1
D
Pf = 12.1 - 15.13 MPa
μ=.6
μ=.5
Failure
ΔPf = 1.1 - 4.13 MPa
τ
σn
σ3
σ2
σ1

Figure 12

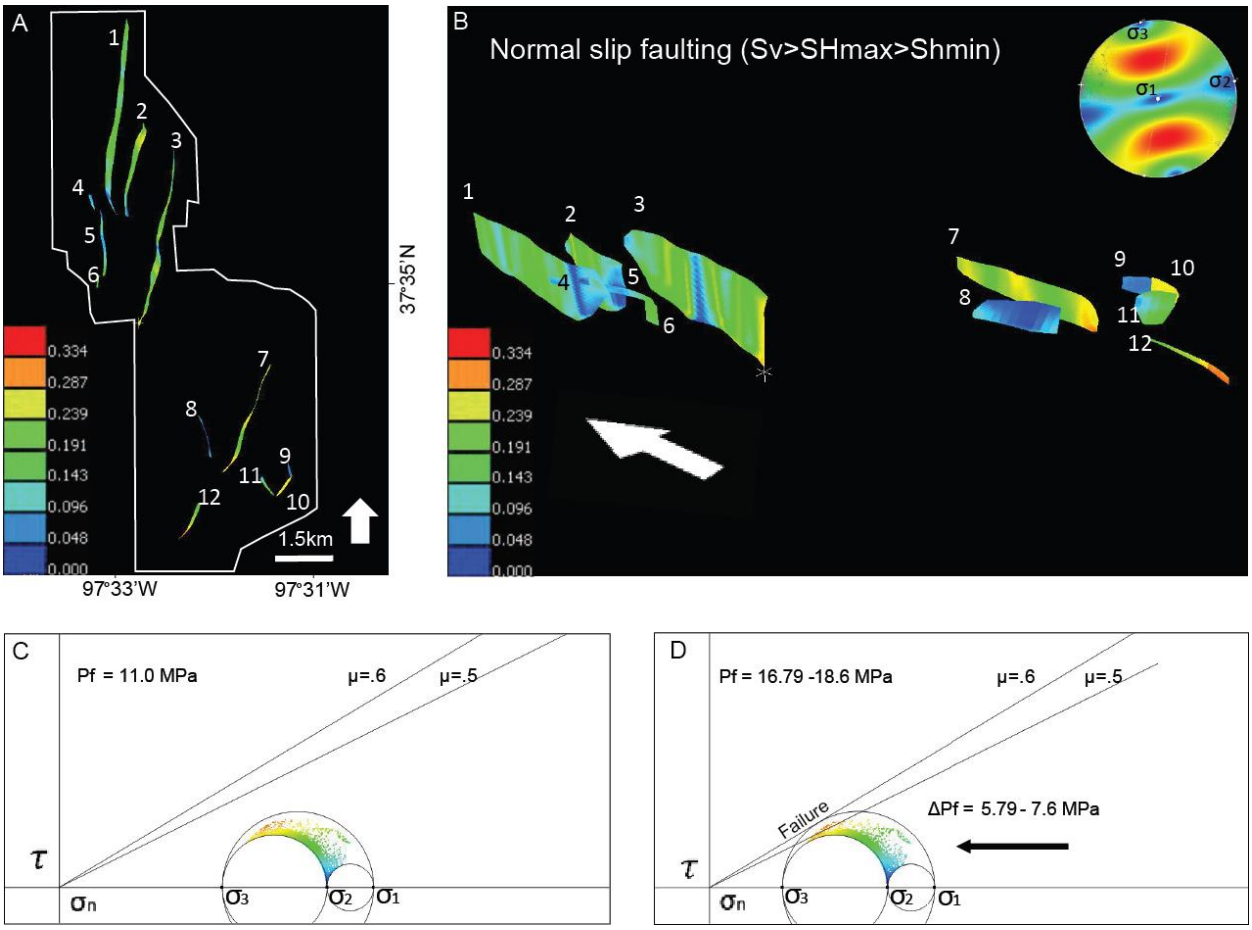
A
1
2
3
4
5
6
7
8
9
10
11
12
0.334
0.287
0.239
0.191
0.143
0.096
0.048
0.000
37°35'N
1.5km
97°33'W
97°31'W
B
Normal slip faulting (Sv>SHmax>Shmin)
σ3
σ1
σ2
C
Pf = 11.0 MPa
μ=.6
μ=.5
τ
σn
σ3
σ2
σ1
D
Pf = 16.79 -18.6 MPa
μ=.6
μ=.5
Failure
ΔPf = 5.79 - 7.6 MPa

Figure 13

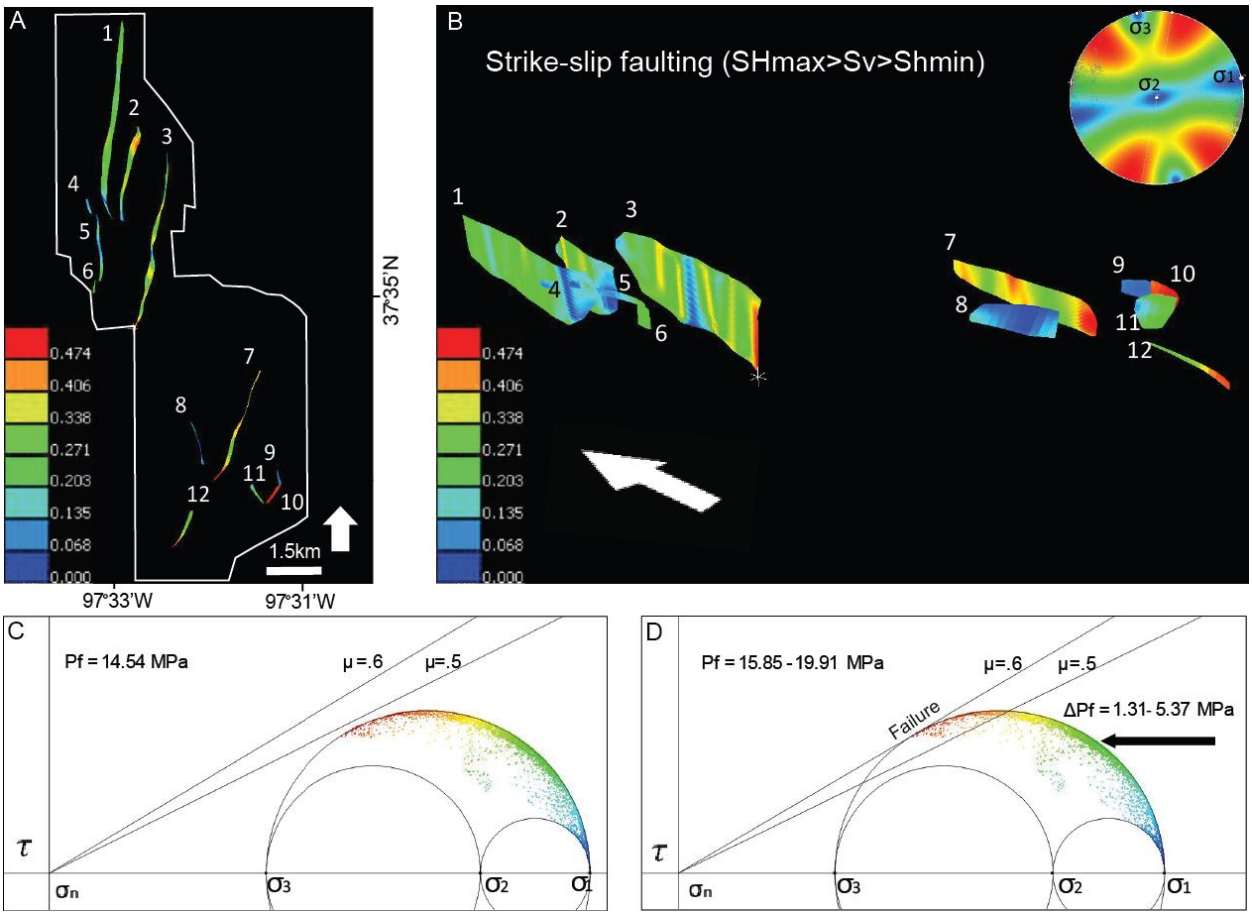
A
1
2
3
4
5
6
7
8
9
10
11
12
0.474
0.406
0.338
0.271
0.203
0.135
0.068
0.000
37°35'N
1.5km
97°33'W
97°31'W
B
Strike-slip faulting (SHmax>Sv>Shmin)
σ3
σ2
σ1
C
Pf = 14.54 MPa
μ=.6
μ=.5
τ
σn
σ3
σ2
σ1
D
Pf = 15.85 - 19.91 MPa
μ=.6
μ=.5
Failure
ΔPf = 1.31- 5.37 MPa

Figure 14

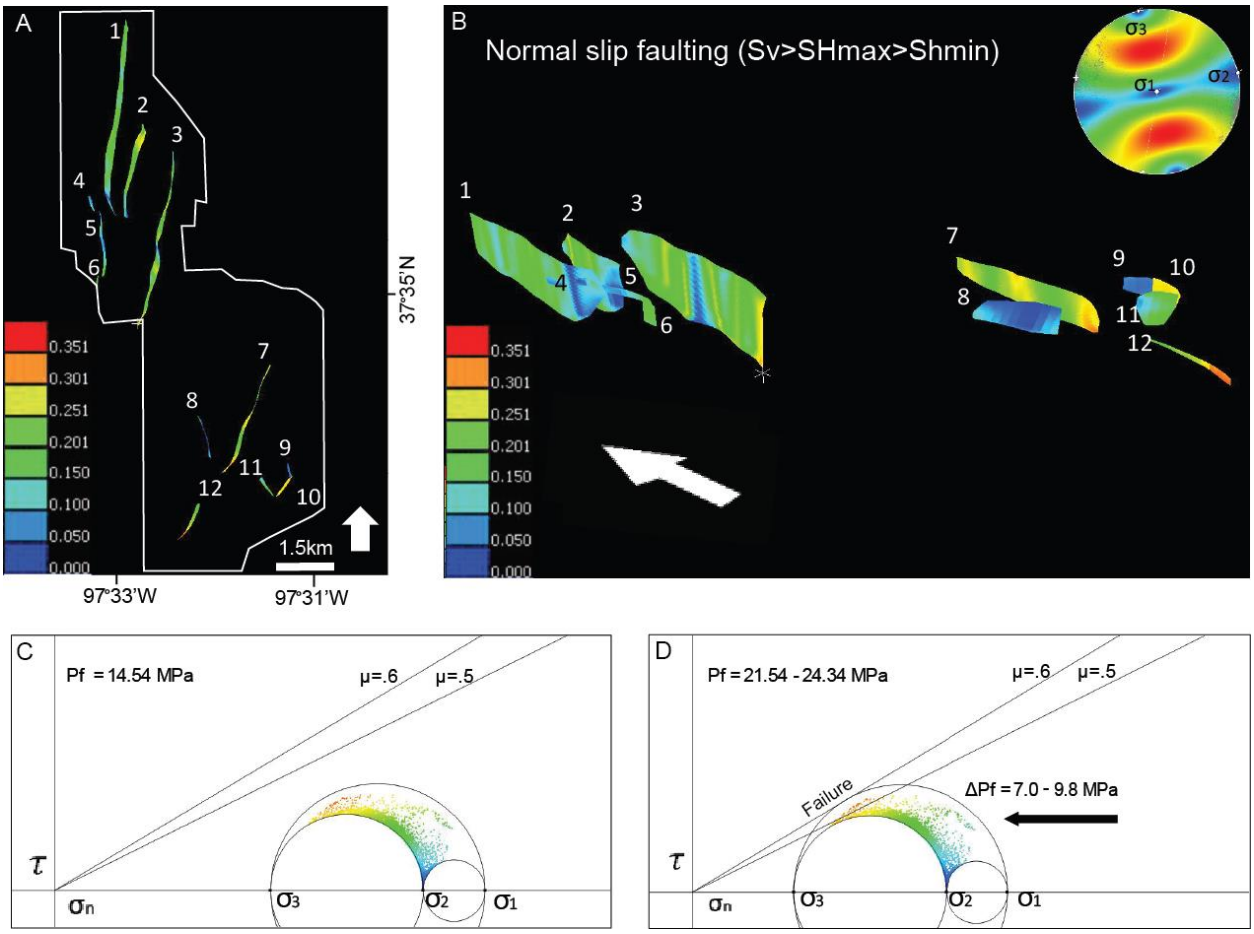
A
1
2
3
4
5
6
7
8
9
10
11
12
0.351
0.301
0.251
0.201
0.150
0.100
0.050
0.000
37°35'N
1.5km
97°33'W
97°31'W
B
Normal slip faulting (Sv>SHmax>Shmin)
σ3
σ1
σ2
C
Pf = 14.54 MPa
μ=.6
μ=.5
τ
σn
σ3
σ2
σ1
D
Pf = 21.54 - 24.34 MPa
μ=.6
μ=.5
Failure
ΔPf = 7.0 - 9.8 MPa
τ
σn
σ3
σ2
σ1

Figure 15

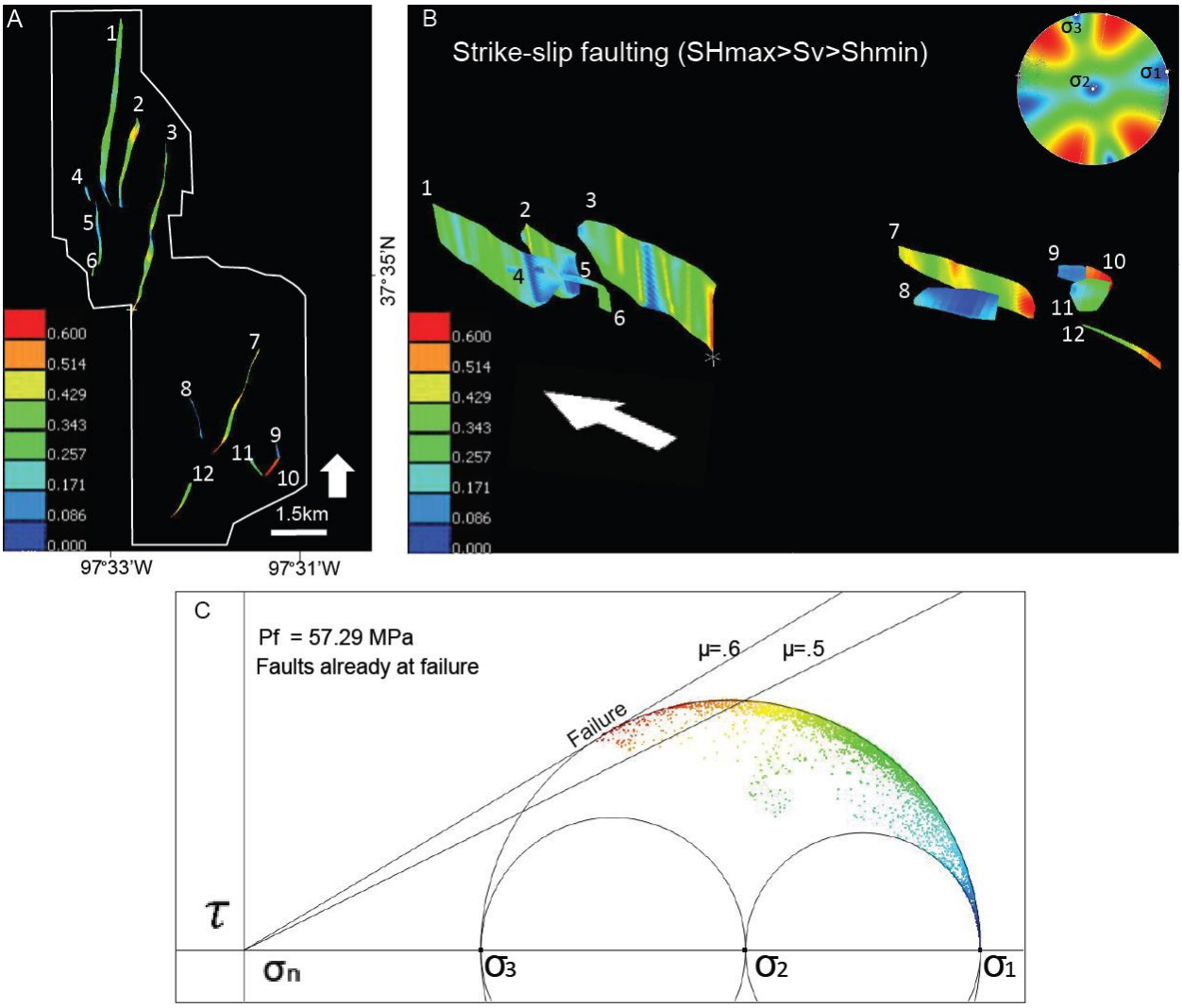
A
1
2
3
4
5
6
7
8
9
10
11
12
0.600
0.514
0.429
0.343
0.257
0.171
0.086
0.000
1.5km
97°33'W
97°31'W
37°35'N
B
Strike-slip faulting (SHmax>Sv>Shmin)
σ3
σ2
σ1
C
Pf = 57.29 MPa
Faults already at failure
μ=.6
μ=.5
Failure
τ
σn
σ3
σ2
σ1

Figure 16

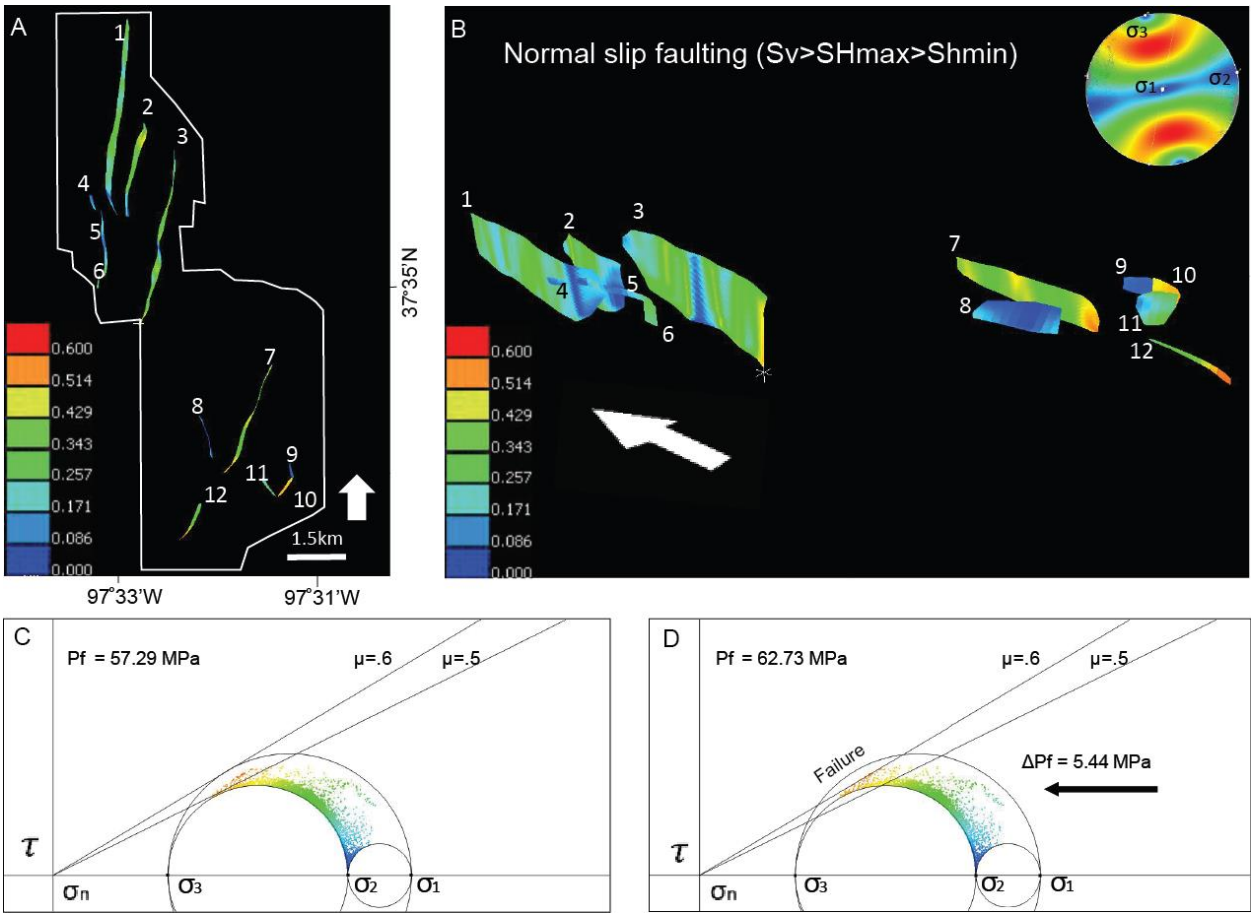
A
1
2
3
4
5
6
7
8
9
10
11
12
0.600
0.514
0.429
0.343
0.257
0.171
0.086
0.000
1.5km
37°35'N
97°33'W
97°31'W
B
Normal slip faulting (Sv>SHmax>Shmin)
σ3
σ1
σ2
C
Pf = 57.29 MPa
μ=.6
μ=.5
τ
σn
σ3
σ2
σ1
D
Pf = 62.73 MPa
μ=.6
μ=.5
Failure
ΔPf = 5.44 MPa
τ
σn
σ3
σ2
σ1

Figure 17

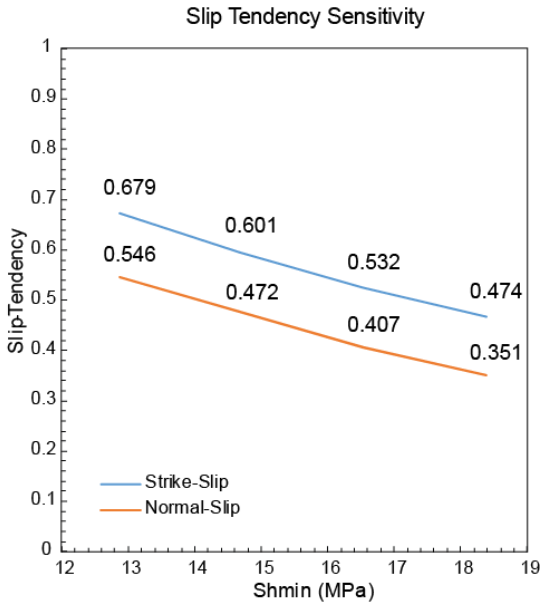
Slip Tendency Sensitivity
Slip-Tendency
Shmin (MPa)
0.679
0.601
0.532
0.474
0.546
0.472
0.407
0.351
Strike-Slip
Normal-Slip

Figure 18